

What can we learn about Reionization astrophysical parameters using Gaussian Process Regression?

PURBA MUKHERJEE ,¹ ANTARA DEY ,^{2,3} AND SUPRATIK PAL ,²

¹*Centre for Theoretical Physics, Jamia Millia Islamia*

New Delhi-110025, India

²*Physics and Applied Mathematics Unit, Indian Statistical Institute*

203, B.T. Road, Kolkata 700 108, India

³*Institute of Physics, Bhubaneswar, Sachivalaya Marg, Odisha 751005, India*

ABSTRACT

Reionization is one of the least understood processes in the evolution history of the Universe, mostly because of the numerous astrophysical processes occurring simultaneously about which we do not have a very clear idea so far. In this article, we use the Gaussian Process Regression (GPR) method to learn the reionization history and infer the astrophysical parameters. We reconstruct the UV luminosity density function using the HFF and early JWST data. From the reconstructed history of reionization, the global differential brightness temperature fluctuation during this epoch has been computed. We perform MCMC analysis of the global 21-cm signal using the instrumental specifications of SARAS, in combination with Lyman- α ionization fraction data, Planck optical depth measurements and UV luminosity data. Our analysis reveals that GPR can help infer the astrophysical parameters in a model-agnostic way than conventional methods. Additionally, we analyze the 21-cm power spectrum using the reconstructed history of reionization and demonstrate how the future 21-cm mission SKA, in combination with Planck and Lyman- α forest data, improves the bounds on the reionization astrophysical parameters by doing a joint MCMC analysis for the astrophysical parameters plus 6 cosmological parameters for Λ CDM model. The results make the GPR-based reconstruction technique a robust learning process and the inferences on the astrophysical parameters obtained therefrom are quite reliable that can be used for future analysis.

Keywords: Cosmology(343) — Reionization(1383) — Cosmic microwave background radiation(322) — Gaussian Processes regression(1930) — Markov chain Monte Carlo(1889) — Luminosity function(942) — Intergalactic medium (813)

1. INTRODUCTION

The epoch of reionization (EoR) represents a crucial period in the evolution history of the Universe, marking the transition from a neutral intergalactic medium (IGM) to one that is fully ionized. This phase, occurring approximately between redshifts $z \approx 6$ and $z \approx 15$, hugely altered the thermal and ionization state of the Universe, setting the stage for the formation and evolution of large-scale cosmic structures (Barkana & Loeb 2001; Choudhury & Ferrara 2005; Furlanetto et al. 2006; Pritchard & Loeb 2012; Kuhlen & Faucher-Giguere 2012). Reionization is primarily driven by the emergence of the first luminous sources, including Population II stars, galaxies, and quasars, which emitted copious amounts of ultraviolet (UV) photons capable of ionizing intergalactic hydrogen. The efficiency of these sources in producing ionizing photons, the fraction of photons that escape into the IGM, and the clumping of the IGM (Madau et al. 1999; Choudhury 2009; Robertson et al. 2013; Bouwens et al. 2017) all play significant roles in shaping the reionization history. These factors collectively influence the reionization power spectrum as well as the global 21-cm signal, both of which serve as key observational probes of this epoch (Pritchard & Loeb

purba16@gmail.com

antaraaddey@gmail.com

supratik@isical.ac.in

2012; Furlanetto et al. 2006). However, despite significant advancements, a complete understanding of the processes that drove reionization and their implications for cosmic evolution remains one of the foremost challenges in contemporary astrophysics.

Along with the lack of sufficient observational data from this epoch, one of the major hurdles towards this direction is a set of astrophysical parameters that govern the epoch of reionization and hence directly impact our understanding of the reionization history and the interpretation of observational data. It is quite a challenging task to constrain these parameters due to their complex interplay and limited observational data, which directly reflects on the (lack of) understanding of the physics of reionization. For instance, the clumping factor C_{HII} , which accounts for the IGM's inhomogeneity, is poorly constrained by observations, with recent simulations suggesting a wide range from 1 to 6 (Iliev et al. 2006; Pawlik et al. 2009; Finlator et al. 2012; Schroeder et al. 2013). Secondly, the number of photons entering the IGM depends on the production rate of Lyman continuum (LyC) photons by stars in galaxies, measured by the ionization efficiency ξ_{ion} , a parameter that counts ionizing photons per unit UV luminosity. Another astrophysical parameter is the escape fraction f_{esc} , which is a measure of the fraction of photons entering the IGM thereby ionizing it, is poorly constrained due to the difficulty in observing the LyC photons beyond $z \sim 2 - 4.5$ (Inoue et al. 2014; Robertson 2021). Earlier studies suggested a low ξ_{ion} and $f_{\text{esc}} \approx 0.2$, fitting more or less well with Cosmic Microwave Background (CMB) data from Planck and Hubble Frontier Fields (HFF) data (Robertson et al. 2013). In contrast, the latest James Webb Space Telescope (JWST) findings indicate a higher ξ_{ion} , especially at $z > 9$, highlighting the degeneracy between ξ_{ion} and f_{esc} (Muñoz et al. 2024; Simmonds et al. 2024; Atek et al. 2024). Recent studies by Kulkarni et al. (2019); Finkelstein et al. (2019); Cain et al. (2021); Katz et al. (2023) have also investigated any possible redshift evolution of f_{esc} . However, Mitra & Chatterjee (2023) suggest that a constant value of f_{esc} between 0.06 and 0.1 for $z \geq 6$ is allowed by existing observational data. Thus, within the Λ CDM framework, magnitude-averaged product of ξ_{ion} and f_{esc} can vary widely depending on the model of reionization, raising significant questions about the validity of cosmological models inferred from reionization data (Hazra et al. 2020; Paoletti et al. 2021; Chatterjee et al. 2021; Dey et al. 2023a,b; Paoletti et al. 2024), which in turn reflects on the inference drawn about the reionization history as a whole.

In light of these widespread uncertainties related to the proper estimation of astrophysical parameters from direct approaches, searches for possible alternative tools that may help in having a somewhat better idea about them from the existing data alone, are natural questions the community has started to ask of late. One such interesting tool is the use of Machine Learning (ML) techniques (Rasmussen & Williams 2006; Takezawa 2006; Harezlak et al. 2018), that can significantly enhance our understanding of the epoch of reionization by developing flexible, data-driven models to analyze observational data. Unlike traditional methods, which depend on the assumption of predefined models that may overlook key details, ML techniques can uncover hidden patterns and relationships in complex data sets. These advanced inference methods can provide a better understanding of the astrophysical parameters, accounting for their variations across different redshifts (Krishak & Hazra 2021; Mitra & Chatterjee 2023), leading to unbiased, model-independent reconstructions of the reionization history and a relatively deeper insight into the underlying physics. In the present article, we seek to elucidate the factors driving reionization and contribute to mapping the Universe's reionization history. As it will turn out, this will stem from a somewhat better hold on the astrophysical parameters through an ML-based learning process.

Further, one of the most exciting probes of the EoR is the spin-flip line of neutral hydrogen, with a rest frame wavelength of 21-cm. Advancements in current instruments and upcoming missions are expected to revolutionize 21-cm cosmology from observational point of view, providing highly significant measurements of both the power spectrum and the global 21-cm brightness temperature signal (Pritchard & Loeb 2012). Currently, the Shaped Antenna measurement of the background RAdio Spectrum (SARAS) (Patra et al. 2013) aims to measure the global sky-averaged 21-cm signal from the cosmic dawn and the EoR using a shaped antenna to capture the redshifted 21-cm line (Singh et al. 2018). In the coming decade, experiments like the Square Kilometre Array (SKA) (de Lera Acedo et al. 2015), Hydrogen Epoch of Reionization Array (HERA) (Abdurashidova et al. 2022) and other significant missions (van Haarlem et al. 2013), will drive advancements in cosmology by detecting the 21-cm neutral hydrogen signal from the early Universe. By employing 21-cm intensity mapping techniques, SKA will track neutral hydrogen in the Universe, yielding comprehensive insights into the post-reionization and reionization epochs, as well as the cosmic dawn, up to a redshift of 30 (Pritchard & Loeb 2012). Our study explores how the ongoing SARAS and next-generation SKA, with their innovative approaches, will enhance our understanding of reionization by reconstructing the reionization history and refining the bounds on the associated astrophysical parameters.

In this work, we intend to enhance the understanding of reionization by examining the effects of various astrophysical parameters on its timeline. We begin by reviewing the theoretical framework that describes the ionization state of the IGM, highlighting significant astrophysical parameters and their connection to observables in sections 2 and 3. Section 4 presents the observational

data relevant to our work. In section 5, we employ an ML algorithm, Gaussian Process Regression¹ (GPR) to perform a Bayesian, non-parametric, model-independent reconstruction (Rasmussen & Williams 2006; Takezawa 2006; Harezlak et al. 2018) of UV luminosity density $\log_{10} \rho_{\text{UV}}$ as a function of redshift, using the current observations from Hubble Frontier Fields (HFF) (Lotz et al. 2017; Schenker et al. 2013; Ellis et al. 2013; McLure et al. 2013; McLeod et al. 2016; Oesch et al. 2018) compiled by (Bouwens et al. 2015b, 2017; Bouwens et al. 2021), early James Webb Space Telescope (JWST) (Harikane et al. 2023), and Subaru HSC’s Great Optically Luminous Dropout Research data (Harikane et al. 2022). GPR, is a non-parametric regression technique that estimates functions based on a Gaussian prior distribution over possible predictions. It provides a flexible, data-driven approach to reconstructing smooth functions from irregularly spaced and heterogeneous data, making it particularly suited for our study. More details on the algorithm, including its historical perspectives and cosmological context, have been discussed previously by some of the authors of the present manuscript in Mukherjee et al. (2024b). A joint evaluation of both the GPR kernel hyperparameters and mean function parameters, allows one to balance the physics-based model with the ML model. Thus, our approach allows for flexible modeling of the evolution of ionizing sources without imposing restrictive parametric forms (Ishigaki et al. 2015, 2018; Adak et al. 2024).

After reconstructing the $\log_{10} \rho_{\text{UV}}$ profile, we then adopt GPR to interpolate between four binned redshifts within $4 < z < 12$, to obtain a smooth and model-independent representation of the reionization history as a function of redshift. For this exercise, we consider the neutral hydrogen fraction measurements (Greig et al. 2017; Davies et al. 2018; Totani et al. 2006; McQuinn et al. 2008; Bolton et al. 2011; Mortlock et al. 2011; Ono et al. 2012; Schenker et al. 2014; Tilvi et al. 2014; Mason et al. 2019) and optical depth τ_{reio} constraints from the Planck 2018 release of CMB observations (Planck Collaboration et al. 2020), in addition to UV luminosity data sets. We undertake a full Bayesian Markov chain Monte Carlo (MCMC) analysis to explore the role of existing data sets for predicting the observationally favoured bounds on the reionization astrophysical parameters. The Bayesian framework of GPR provides valuable advantages in this regard, both as a maximum likelihood estimator (MLE) and as an interpolant between redshift bins.

In what follows, we detail our methodology for analyzing the global 21-cm signal and the reionization power spectrum within the framework of the Λ CDM cosmological model. For the global 21-cm signal ΔT_b , we generate a mock ΔT_b vs z data, assuming the instrumental specifications of SARAS (Patra et al. 2013), considering the best-fit values of these astrophysical parameters obtained using the existing data sets. For the power spectrum analysis, we use the instrumental specifications of SKA to generate a mock data set (Dewdney & Braun 2016), using the Planck 2018 best-fit Λ CDM model. We make prior modifications in CLASS (Blas et al. 2011) to incorporate the contribution from the GP reconstructed reionization history profile (instead of the inbuilt tanh reionization model), to compare both the cases and reflect on their outcomes. In the final step, we conduct a comprehensive Bayesian MCMC analysis to investigate how SARAS and upcoming SKA will aid in probing the astrophysical parameters of reionization. We summarize our findings in section 6, and make some concluding remarks in section 7.

2. ASTROPHYSICAL PARAMETERS AND THE ROLE OF MACHINE LEARNING

The ionization equation describes the time evolution of the volume filling factor of ionized hydrogen in the intergalactic medium, Q_{HII} , by a first-order ordinary differential equation,

$$\frac{dQ_{\text{HII}}}{dt} = \frac{\dot{n}_{\text{ion}}}{\langle n_{\text{H}} \rangle} - \frac{Q_{\text{HII}}}{t_{\text{rec}}}. \quad (1)$$

The source term \dot{n}_{ion} is characterized by the rate of production of ionizing photons, which depends on (i) the UV luminosity density function ρ_{UV} , (ii) the efficiency of the source to produce ionizing photons ξ_{ion} , (iii) the fraction of photons that escape into the IGM f_{esc} . It is defined as,

$$\dot{n}_{\text{ion}} = \rho_{\text{UV}} \langle f_{\text{esc}} \xi_{\text{ion}} \rangle, \quad (2)$$

where $\langle f_{\text{esc}} \xi_{\text{ion}} \rangle$ is a magnitude-averaged product. The sink term in the ionization equation accounts for the recombination process in the IGM. The recombination time t_{rec} , given by

$$t_{\text{rec}} = \left[C_{\text{HII}} \alpha_B(T) \left(1 + \frac{Y_p}{4X_p} \right) \langle n_{\text{H}} \rangle (1+z)^3 \right]^{-1} \quad (3)$$

where n_{H} , n_{He} , n_{HII} are the number densities of hydrogen, helium, and ionized hydrogen, is determined by the recombination coefficient $\alpha_B(T)$ and the clumping factor C_{HII} . Here, X_p , Y_p are the primordial mass fractions of hydrogen and helium. The

¹ <https://gaussianprocess.org/gpml/>

C_{HII} accounts for the inhomogeneity of the IGM, and is not very well constrained from observations. The IGM temperature T is fixed at 20,000 K.

From the solution of the ionization Eq. (1), the Thomson scattering optical depth is defined as,

$$\tau = \int \frac{c(1+z)^2}{H(z)} Q_{\text{HII}}(z) \langle n_{\text{H}} \rangle \sigma_{\text{T}} \left(1 + \eta \frac{Y_p}{4X_p} \right) dz, \quad (4)$$

where helium is assumed to be singly-ionized for $z > 4$ ($\eta = 1$) and doubly-ionized for $z < 4$ ($\eta = 2$) (Kuhlen & Faucher-Giguere 2012).

Thus, the astrophysical parameters play a crucial role in driving the reionization history as well as in constraining the underlying cosmological model parameters therefrom. However, in the absence of sufficient information about these astrophysical parameters, either from the 21-cm signal or complementary probes, their range of allowed values remains significantly wide. As a result, it is unlikely to draw reliable conclusions about the cosmological model and the reionization history. So, to have a better understanding of the scenario, the community has to wait for improved data, hopefully leading to more precise values of the astrophysical parameters. Alternatively, one can utilize statistical/numerical tools to predict the nature of reionization history in a non-parametric way by making use of the existing data from complimentary probes like HST and JWST, and infer the astrophysical parameters therefrom. Herein lies the major role of ML techniques as an interesting route to progress even with currently available data sets.

In this work, we employ a particular ML technique- Gaussian Process Regression (GPR)- to infer the astrophysical parameters that would in turn help us have a better understanding of the reionization history as well as a better hold on the cosmological parameters in the reionization era. To this end, we attempt to first reconstruct the UV luminosity density using GPR in a non-parametric way with the UV LF data. Subsequently, we will use the reconstructed values of $\log_{10} \rho_{\text{UV}}$, interpolated at four binned redshifts within $4 < z < 12$, in combination with the volume-averaged neutral hydrogen fraction (Q_{HII}), and the Thomson optical depth (τ_{reio}) measurements, to derive a model-independent reionization history profile as a function of redshift and infer the astrophysical parameters $\langle f_{\text{esc}} \xi_{\text{ion}} \rangle$ and C_{HII} , respectively.

3. 21CM-COSMOLOGY AND OBSERVABLES

In this section, extend our analysis to the yet-unexplored directions on reionization studies. This is materialized by considering the global 21-cm signal and 21-cm power spectrum, exploring their potential in inferring the reionization physics.

3.1. Global Brightness Temperature Fluctuation

The key observable in 21-cm cosmology is the global brightness temperature fluctuation, which is the difference between the spin temperature (related to the neutral hydrogen number densities in different atomic levels) and the background temperature. The total brightness temperature at redshift z is given by the temperature of the background radiation field, with some fraction of it absorbed and re-emitted due to 21-cm hyperfine transitions in neutral hydrogen atoms. The properties of HI in absorption and emission are described by the spin temperature T_s and the optical depth τ (Pritchard & Loeb 2012; Furlanetto et al. 2006):

$$T_b = T_s(1 - e^{-\tau}) + T_{\gamma}e^{-\tau}. \quad (5)$$

Due to the low probability of a 21-cm transition, the optical depth is typically small. The differential brightness temperature can thus be written as linear in τ :

$$\Delta T_b = \frac{T_s - T_{\gamma}}{1+z} (1 - e^{-\tau}) \approx \frac{T_s - T_{\gamma}}{1+z} \tau. \quad (6)$$

The optical depth produced by a patch of neutral hydrogen at the mean density and with a uniform 21-cm spin temperature T_s ,

$$\tau = 9.0 \times 10^{-3} \left(\frac{T_{\text{CMB}}}{T_s} \right) \left(\frac{\Omega_{\text{b}} h}{0.03} \right) \left(\frac{\Omega_{\text{m}}}{0.3} \right)^{-1/2} \left(\frac{1+z}{10} \right)^{1/2}. \quad (7)$$

The Lyman- α (Ly α) and X-ray radiation backgrounds during the epoch of reionization are anticipated to be strong enough to equalize the spin temperature T_s with the gas temperature and heat up the cosmic gas well above the CMB temperature (Madau et al. 1997). In these circumstances, the observed 21-cm brightness temperature T_b , in relation to the CMB temperature T_{γ} , becomes independent of T_s . Consequently, T_b (hereafter measured relative to T_{γ}) is given by (Morandi & Barkana 2012)

$$\Delta T_b = (T_s - T_{\gamma})(1 - e^{-\tau}) Q_{\text{HI}} \approx T_{21} \left(\frac{1+z}{10} \right)^{1/2} Q_{\text{HI}}, \quad (8)$$

where $T_{21} = 9.0 \times 10^{-3}(\Omega_b h/0.03)(\Omega_m/0.3)^{-1/2} T_{\text{CMB}} = 27.2 \text{ mK}$ and Q_{HI} is the neutral hydrogen fraction. We focus solely on the cosmic mean neutral or ionized fraction and disregard spatial fluctuations in the 21-cm signal caused by density and peculiar velocity variations.

3.2. Power Spectrum

The difference between the 21-cm temperature $T_b(\mathbf{x})$ and the average temperature $\bar{T}_b(z)$ at a given redshift can be calculated at any spatial point and is denoted by $\Delta T_b(\mathbf{x})$. Its Fourier transform is indicated as $\Delta T_b(\mathbf{k})$. The two-point correlation function of 21-cm temperature fluctuations at redshift z is written as (Muñoz et al. 2017)

$$\Delta T_b(\mathbf{k})\Delta T_b(\mathbf{k}') \equiv P_{21}(\mathbf{k}, z)(2\pi)^3\delta_D(\mathbf{k} - \mathbf{k}'), \quad (9)$$

with

$$P_{21}(\mathbf{k}, z) = [\mathcal{A}(z) + \bar{T}_b(z)\mu^2]^2 P_{\text{HI}}(\mathbf{k}, z), \quad (10)$$

here, $\mathcal{A}(z) = dT_{21}/d\delta_b$ indicates a function of z , $\mu \equiv k_{||}/k$ is the cosine of the angle between the line-of-sight $k_{||}$ and the total wave vector $k = |\mathbf{k}|$, and P_{HI} is the power spectrum for the perturbations in neutral hydrogen density, which is related to matter power spectrum $P_m(\mathbf{k}, z)$ with a bias b_{HI} . We have used the bias model $b_{\text{HI}}(z) = \beta_0 (0.904 + 0.135(1+z)^{0.198\beta_1})$, where β_0 and β_1 are treated as nuisance parameters (Sprenger et al. 2019).

The spin temperature T_s during the EoR is coupled to the gas temperature through the Wouthuysen-Field effect (Wouthuysen 1952; Hirata 2006). The star formation heats the gas, which give rise the spin temperature above the CMB temperature T_γ , making the 21-cm line appear in emission. In this epoch, we can express the factors in Eq. (10) as, (Muñoz et al. 2017)

$$\mathcal{A}(z) = \bar{T}_{21}(z) = 27.3 \text{ mK} \times \bar{x}_{\text{H}} \frac{T_s - T_\gamma}{T_s} \left(\frac{1+z}{10} \right)^{1/2}, \quad (11)$$

here we can drop the temperature factor since $T_s \gg T_\gamma$, and \bar{x}_{H} represents the mean neutral hydrogen fraction

Assuming an antenna array with a baseline D_{base} uniformly covered to a fraction $f_{\text{cover}} \leq 1$ and an observation time of t_o , the instrumental-noise power spectrum in k -space is given by (Zaldarriaga et al. 2004; Tegmark & Zaldarriaga 2009)

$$P_{21}^N(z) = \frac{\pi T_{\text{sys}}^2}{t_o f_{\text{cover}}^2} \chi^2(z) y_\nu(z) \frac{\lambda^2(z)}{D_{\text{base}}^2}, \quad (12)$$

In this context, $\lambda(z)$ is the 21-cm transition wavelength corresponding to redshift z , $y_\nu(z) = 18.5\sqrt{(1+z)/10} \text{ Mpc/MHz}$ serves as the conversion function from frequency ν to $k_{||}$, and the system temperature T_{sys} is predominantly determined by galactic synchrotron emission, characterized as (de Oliveira-Costa et al. 2008)

$$T_{\text{sys}} = 180 \text{ K} \times \left(\frac{\nu}{180 \text{ MHz}} \right)^{-2.6}. \quad (13)$$

Combining all these pieces of information, the observed power spectrum looks like (Sprenger et al. 2019; Dey et al. 2023b)

$$P_{21,\text{obs}}(\mathbf{k}, \mu, z) = f_{\text{AP}}(z) \times f_{\text{res}}(k, \mu, z) \times f_{\text{RSD}}(\hat{k}, \hat{\mu}, z) \times P_{21}(\mathbf{k}, z) + P_{21}^N(z), \quad (14)$$

where $P_{21}(\mathbf{k}, z)$ denotes the 21-cm power spectrum. In the above formula, we have applied the flat-sky approximation, which provides a specific definition of the line-of-sight distance vector \vec{r} and Fourier modes. This approximation breaks the isotropy along the observer's line of sight but retains the symmetry perpendicular to it. The coordinate relations are as follows: $k = |\vec{k}|$, $\mu = \frac{\vec{k} \cdot \vec{r}}{kr}$, with the parallel component of the mode being $k_{||} = \mu k$ and the perpendicular component being $k_{\perp} = k\sqrt{1 - \mu^2}$.

4. DATA SETS

In the process of learning the reionization history, we have two-fold goals: (i) to find out the present constraints from a couple of cosmological data sets that also help in the reconstruction process and (ii) to forecast on the astrophysical parameters along with the cosmological parameters from the 21-cm power spectra.

For current constraints, the data sets used are the following:

- The UV luminosity density ρ_{UV} data, derived by integrating the UV LF, $\Phi(M_{\text{UV}})$, as $\rho_{\text{UV}} = \int_{M_{\text{trunc}}}^{-\infty} \Phi(M) L(M) \text{d}M$, where $L(M)$ represents the luminosity at a given absolute magnitude M_{UV} . The integration limit is set at a conservative truncation magnitude $M_{\text{trunc}} = -17$, corresponding to the minimum observed halo mass that can host star-forming faint galaxies. The estimation of ρ_{UV} relies on an accurate characterization of the LF profile, which describes the number density of star-forming galaxies at different luminosities, modeled via the *Schechter* function (*Schechter 1976*). Herein, we use two compilations of UV luminosity from various deep-field surveys,
 - **UV17(A)**: The derived UV LF density data ([Bouwens et al. 2015a, 2017](#)) at $z \sim 4-10$ from HFF observations² ([Lotz et al. 2017](#)), illustrated in Fig. 1(b).
 - **UV17(B)**: The UV LF data for $z \sim 2 - 7$, derived in [Adak et al. \(2024\)](#) using the HUDF, HFF, and CANDELS fields, compiled by ([Bouwens et al. 2015a; Ishigaki et al. 2018](#)). For $z \sim 4 - 7$, we incorporate data from the Hyper Suprime-Cam (HSC) Subaru Strategic Program (SSP) survey ([Harikane et al. 2022](#)). For $z \sim 8 - 10$, we consider the derived LF obtained by [Bouwens et al. \(2023\)](#); [Adak et al. \(2024\)](#) and early JWST data at $z \sim 9$ and 12 ([Harikane et al. 2023](#)). For visualization, see Fig. 1(c).
- **QHII**: Neutral hydrogen fraction (Q_{HII}) measurements from multiple probes, illustrated in Figs. 3(a)-(b), providing complementary insights into the patchy nature of reionization across cosmic epochs.
 - Ly α emission from galaxies ([Ono et al. 2012; Schenker et al. 2014; Tilvi et al. 2014; Mason et al. 2019](#))
 - Damping wing absorption signatures of gamma-ray bursts ([Totani et al. 2006; McQuinn et al. 2008](#))
 - Dark gap in quasar spectra, indicating neutral intergalactic medium regions ([McGreer et al. 2015](#))
 - Ionized proximity zones near high redshift quasars, to estimate the surrounding ionization state ([Mortlock et al. 2011; Bolton et al. 2011](#))
- **Planck**: The Thomson scattering optical depth constraints $\tau_{\text{reio}} = 0.054 \pm 0.007$ from Planck 2018 release of CMB observation ([Planck Collaboration et al. 2020](#)), as an integrated measure of the reionization history (illustrated via dashed lines with shaded regions in Fig. 2). We adopt the mean and the 1σ confidence limit of τ_{reio} from the Planck TT-TEEE+lowE+lensing likelihood as summary statistics. Instead of using the full Planck MCMC chains, we incorporate this constraint as a Gaussian prior on τ_{reio} , ensuring consistency with CMB-derived reionization models.

On the other hand, for future forecasts from 21-cm observables, viz. the global brightness temperature fluctuations and power spectra, we make use of the following data sets:

- **SARAS**: Mock data generated from the instrumental specifications of the global 21-cm mission ([Patra et al. 2013](#)), incorporated alongside the existing observational datasets. For a visualization of the generated mock ΔT_b vs z , one can refer to Fig. 4(d).
- **Planck**: Mock Planck 2018 data ([Planck Collaboration et al. 2020; Sprenger et al. 2019](#)), generated for forecast analysis, making it suitable for combination with other future experiments using `MontePython` ([Audren et al. 2013; Brinckmann & Lesgourges 2019](#)). It is derived by sampling from the posterior distribution of Planck MCMC chains, ensuring realistic uncertainties and statistical properties, incorporating the theoretical CMB power spectra predictions, instrumental noise, and observational constraints.
- **Ly α** : MIKE-HIRES Lyman- α forest dataset ([Viel et al. 2013](#)), obtained from QSO spectra measured with the HIRES/KECK and MIKE/Magellan spectrographs, has been used. These observations span redshift bins $z = 5.0$ and $z = 5.4$, with spectral resolution of 13.6 km/s (HIRES) and 6.7 km/s (MIKE), and are binned into 10 k -bins over the range $0.001 - 0.08$ s/km. We impose a conservative cut on the flux power spectrum, including only measurements with $k > 0.005$ s/km to minimize potential systematic uncertainties from continuum fitting at large scales.
- **SKA**: Simulated data using the instrumental specifications of SKA-Low ([Dewdney & Braun 2016](#)), generated incorporating noise modeling and conservative foreground mitigation strategies to mimic realistic survey conditions. Our key observable is the 21-cm power spectrum, to forecast the expected 21-cm signal from reionization epochs, enabling constraints on reionization parameters and astrophysical models.

² <http://www.stsci.edu/hst/campaigns/frontier-fields/>

5. METHODOLOGY

5.1. Reconstructing the UV luminosity density

The evolution of the UV luminosity density with redshift can be obtained by parametric (Yu et al. 2012; Ishigaki et al. 2015, 2018; Adak et al. 2024) and non-parametric free-form methods (Hazra et al. 2020; Paoletti et al. 2021) to determine n_{ion} . Recently, a model-independent reconstruction of ρ_{UV} by (Krishak & Hazra 2021) invalidates the single power-law form (Yu et al. 2012), as it fails to account for the decline at $z \sim 8$, resulting in an incorrect Thomson scattering optical depth. Therefore, the assumption of a parametric logarithmic double power law (Ishigaki et al. 2015, 2018), given by

$$\rho_{\text{UV}}(z) = \frac{2\rho_{\text{UV},z=z_1}}{10^{a(z-z_1)} + 10^{b(z-z_1)}}, \quad (15)$$

to describe the UV LF profile is a better ansatz, characterised by four distinct parameters, namely - the amplitude ($\rho_{\text{UV},z=z_1}$), two tilts (a, b) and the redshift (z_1) at which the tilt in the power changes.

While parametric methods are useful, the functional form restricts their ability to address the data in several instances [see (Yu et al. 2012; Ishigaki et al. 2018; Adak et al. 2024)]. So, a more robust approach is a non-parametric reconstruction which attempts to reconstruct the cosmic reionization history directly from the observational data. In this article, we use GPR (Rasmussen & Williams 2006; Seikel et al. 2012; Shafieloo et al. 2012; Mukherjee 2022; Shah et al. 2023; Mukherjee et al. 2024b) for a Bayesian, non-parametric reconstruction (Takezawa 2006; Harezlak et al. 2018) of luminosity density in a model-independent manner.

5.2. Gaussian Process Framework

A Gaussian Process (GP) is a collection of random variables such that the joint distribution of any finite subset of it is described by a multivariate Gaussian. It is characterized by a mean function $\mu(\mathbf{x})$ and covariance function $k(\mathbf{x}, \mathbf{x}')$, where for a real process $f(\mathbf{x})$, we have $\mu(\mathbf{x}) = \mathbb{E}[f(\mathbf{x})]$, and $k(\mathbf{x}, \mathbf{x}') = \mathbb{E}[(f(\mathbf{x}) - \mu(\mathbf{x}))(f(\mathbf{x}') - \mu(\mathbf{x}'))]$.

For a finite set of training points $\mathbf{x} = \{x_i\}$, a function $f(\mathbf{x})$ evaluated at each x_i can be represented by a random variable with a Gaussian distribution, such that the vector $\mathbf{f} = \{f_i\}$ has a multivariate Gaussian distribution given as $\mathbf{f} \sim \mathcal{N}(\mu(\mathbf{x}), C(\mathbf{x}, \mathbf{x}))$, where C is the covariance matrix characterized by the kernel or covariance function $k(x_i, x_j)$, which gives the covariance between two random variables x_i and x_j respectively.

For our analysis, we choose the Radial Basis Function (RBF) kernel, represented as $k(x_i, x_j) = \sigma_f \exp\left[-\frac{(x_i-x_j)^2}{2l^2}\right]$, with the correlation length l and amplitude σ_f . The logarithmic double power law parametrization, given in Eq. (15) is considered a mean function, whose parameters are jointly constrained with the kernel hyperparameters, marginalizing the log-likelihood via a Bayesian MCMC analysis with emcee (Foreman-Mackey et al. 2013). The constraints on the kernel hyperparameters and parameters governing the mean function are shown in Fig. 1(a).

We undertake this exercise for both UV17(A) and UV17(B) compilations of the luminosity density data as the training set. Although our reconstruction method is somewhat in the same vein of Krishak & Hazra (2021), where the mean function is fixed to the best-fit values obtained by χ^2 minimization, our novelty lies in simultaneously training the parameters governing the GP mean function and the kernel hyperparameters to obtain the predicted UV luminosity density profile, which helps the predictions arise from a symbiotic environment and hence is expected to generate more realistic outcome of the learning process.

5.3. Learning the reionization history

On having reconstructed the profile of UV luminosity density in a model-independent way, we now re-define the values of $\log_{10} \rho_{\text{UV}}$ in four distinct equidistant nodes in the range $4 < z < 12$. Our approach is akin to Gerardi et al. (2019), where this range is selected to fully encompass available UV17(A) and UV17(B) data sets. The values of the UV luminosity density at these four nodes i.e., $\log_{10} \rho_{1-4}$ are taken as free parameters in MCMC sampling, employing emcee (Foreman-Mackey et al. 2013), to learn the reionization history by solving the ionization Eq. (1) using this model-independent form. At each MCMC step, these points serve as training data for GP regression. Hence, GP reconstruction yields samples of the history of UV luminosity densities, based on the training input configurations.

For this full Bayesian analysis, we take into account different combinations of the existing data sets, described in Sec. 4. In the ionization equation, we treat $\langle f_{\text{esc}} \xi_{\text{ion}} \rangle$ as a single parameter by incorporating f_{esc} into ξ_{ion} (Dayal & Ferrara 2018). Following Price et al. (2016), we apply a uniform prior on $\log_{10} \xi_{\text{ion}} \in \mathcal{U}[23.5, 27.5]$ in units of $\log_{10} [\text{Hz erg}^{-1}]$. The clumping factor is initially treated as a free parameter with a uniform prior, setting an upper bound at $C_{\text{HII}} \leq 10$. Later on, it is kept fixed at $C_{\text{HII}} = 5$, similar to Krishak & Hazra (2021). This helps us explore the outcome of both cases for a comparative analysis.

In the final stage, we modify the public version of the Boltzmann solver code `CLASS` (Blas et al. 2011), where this reconstructed reionization history is supplied as an input within the `thermodynamics.c` module, in place of the Planck tanh reionization model. This helps us consistently overcome any dependence of the baseline reionization model on the estimated parameters and search for possible consequences of the present learning method. For this we undertake a joint MCMC analysis on the 6 Λ CDM cosmological parameters and 2 reionization astrophysical parameters using `MontePython` (Audren et al. 2013; Brinckmann & Lesgourgues 2019) by generating mock data for the upcoming 21-cm SKA mission along with some other data sets mentioned in Sec. 4. We subsequently analyze the errors and correlations of the different model parameters.

5.4. *Advancements over previous works*

Our work advances from the earlier works in this direction (see, for example, Krishak & Hazra (2021); Chatterjee et al. (2021); Paoletti et al. (2021); Adak et al. (2024)) by multiple folds:

- We employ GPR by simultaneously training the parameters governing the GP mean function and the kernel hyperparameters (instead of fixing the mean function to the best-fit values) to obtain the predicted UV LF density profile.
- Along with other astrophysical parameters, we keep the clumping factor C_{HII} as a free parameter in MCMC analysis (and compare with earlier studies with a fixed value $C_{\text{HII}} = 5$).
- We consider both HFF and JWST as the reconstruction training data sets (along with possible combinations of other data sets), followed by a thorough, methodical comparative analysis between their role in constraining the astrophysical parameters and hence in deriving reionization history.
- We extend our analysis to the yet-unexplored directions on the applications of GPR in reionization. This is materialized by considering, separately, the global 21-cm signal (from SARAS) and 21-cm power spectrum (from SKA), which helps explore their role in inferring the reionization physics.
- And finally, we modify the Boltzmann solver code `CLASS` (Blas et al. 2011) to accommodate our reconstructed reionization history into the MCMC code `MontePython` (Audren et al. 2013; Brinckmann & Lesgourgues 2019).

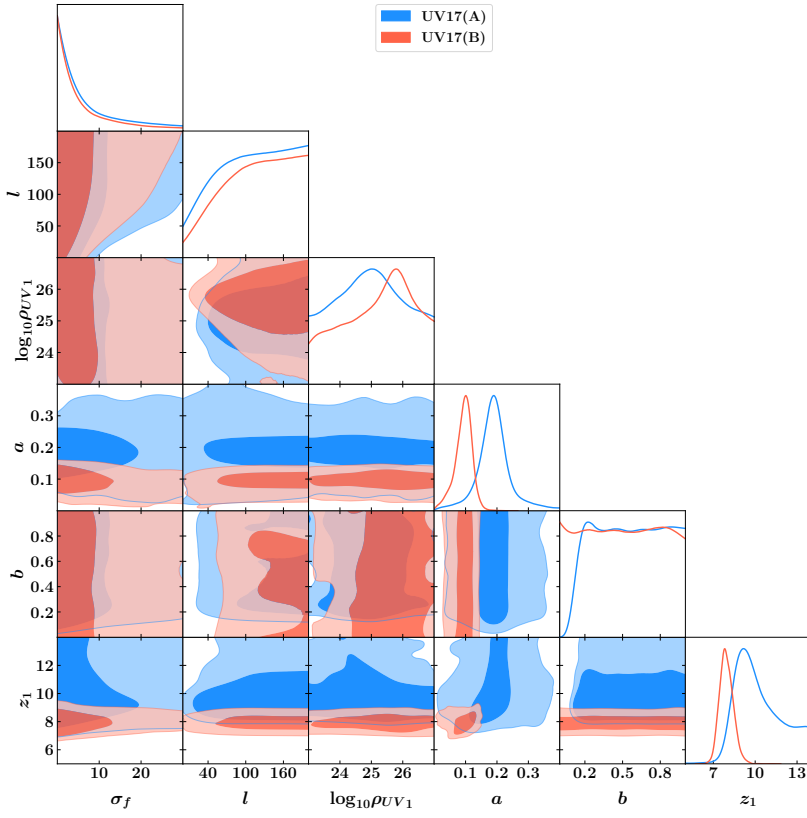
Thus, our findings are expected to have important implications for understanding the nature and distribution of the first light sources and their role in shaping the early Universe.

6. RESULTS & DISCUSSIONS

6.1. *Analysis with existing datasets*

Following the methodology described in Sec. 5.1, we reconstruct the UV luminosity density as a function of redshift in the range $4 < z < 12$ employing GPR on the UV17(A) and UV17(B) data sets. Fig. 1(b) and (c) illustrate the reconstructed UV luminosity density profile as a function of redshift for both UV17(A) and UV17(B) compilation, respectively. The solid blue curve represents the GP reconstructed mean curve, and the shaded regions correspond to the 1σ and 2σ uncertainties associated with the reconstructed curve. The black dotted lines give the best-fit curves assuming the logarithmic double power-law parametric form to model the $\log_{10} \rho_{\text{UV}}$ data. The predicted logarithmic double power-law evolution as a mean function for GPR is shown with red dashed lines. Our findings indicate that the logarithmic double power law model is consistent with the reconstructed GP function and the UV17(A) and UV17(B) data within the redshift range $4 < z < 8$. For $z > 9$, the mean reconstructed curve deviates from the best-fit values. However, this deviation is included within 1σ for the UV17(A) data and 2σ for the UV17(B) data. In the case of UV17(B) data, the reconstructed UV luminosity curve excludes the $z = 9$ and $z = 10$ JWST $\log_{10} \rho_{\text{UV}}$ data points.

With this reconstructed UV luminosity profile, we proceed to trace the evolution of the ionization fraction Q_{HII} , following the methodology described in Sec. 5.3. For this we adopt four equidistant redshift nodes at $z_1 = 4$, $z_2 = 6$, $z_3 = 8$ and $z_4 = 10$, where the values of logarithmic UV luminosity densities are redefined as $\log_{10} \rho_1$, $\log_{10} \rho_2$, $\log_{10} \rho_3$ and $\log_{10} \rho_4$ respectively. We make use of Eq. (1) to solve for Q_{HII} where the reconstructed values of the UV luminosity densities (at the 4 redshift nodes) are treated as free parameters during the Bayesian MCMC analysis. The entire exercise is undertaken employing different data sets, mentioned in Sec. 4, namely, UV17(A) & UV17(B) in combination with QHII Ly α and Planck τ_{reio} data. Fig. 2(a)-(b) shows the 2D-confidence contours and 1D-marginalized posteriors for the relevant parameters upon MCMC done using the joint UV17(A)+QHII (in blue) and UV17(B)+QHII (in red) data sets. The black dashed line and shaded region represent the Planck baseline best-fit with 1σ CL. Similarly, Fig. 2(c)-(d) depicts the same for UV17(A)+QHII+Planck (in blue) and



(a) Trained MCMC samples of kernel hyperparameter and parameters governing the mean function for GPR

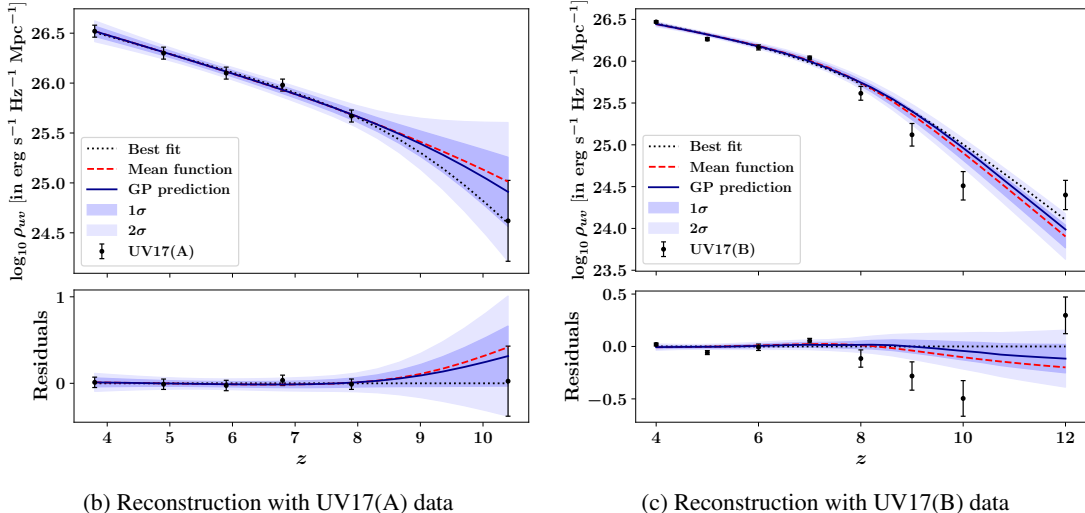


Figure 1. The reconstructed UV luminosity density function in the redshift range $z \sim 4 - 12$ obtained from Gaussian Process regression using the UV17(A) and UV17(B) data.

UV17(B)+QHII+Planck (in red) combinations. It should be noted that, in panels (a) and (c) of Fig. 2, the clumping factor C_{HII} is treated as a free parameter during MCMC, whereas the panels (b) and (d) shows the case when the value of the clumping factor is kept fixed at $C_{\text{HII}} = 5$ respectively. For both (a) and (c), we find that the parameters $\log_{10} \langle f_{\text{esc}} \xi_{\text{ion}} \rangle$ and C_{HII} are positively correlated. This feature indicates an anti-correlation with t_{rec} , i.e., a reduction in $\langle f_{\text{esc}} \xi_{\text{ion}} \rangle$ lowers the source term, which is only offset by a longer recombination period to maintain ionization [see Gorce et al. (2018); Mason et al. (2019); Paoletti et al. (2021); Krishak & Hazra (2021)]. The values of UV luminosity densities at redshift points z_1 , z_2 , and z_4 differ greatly between the two different combinations of the data sets. However, at z_3 , the average values are very similar, where the inclusion of early JWST

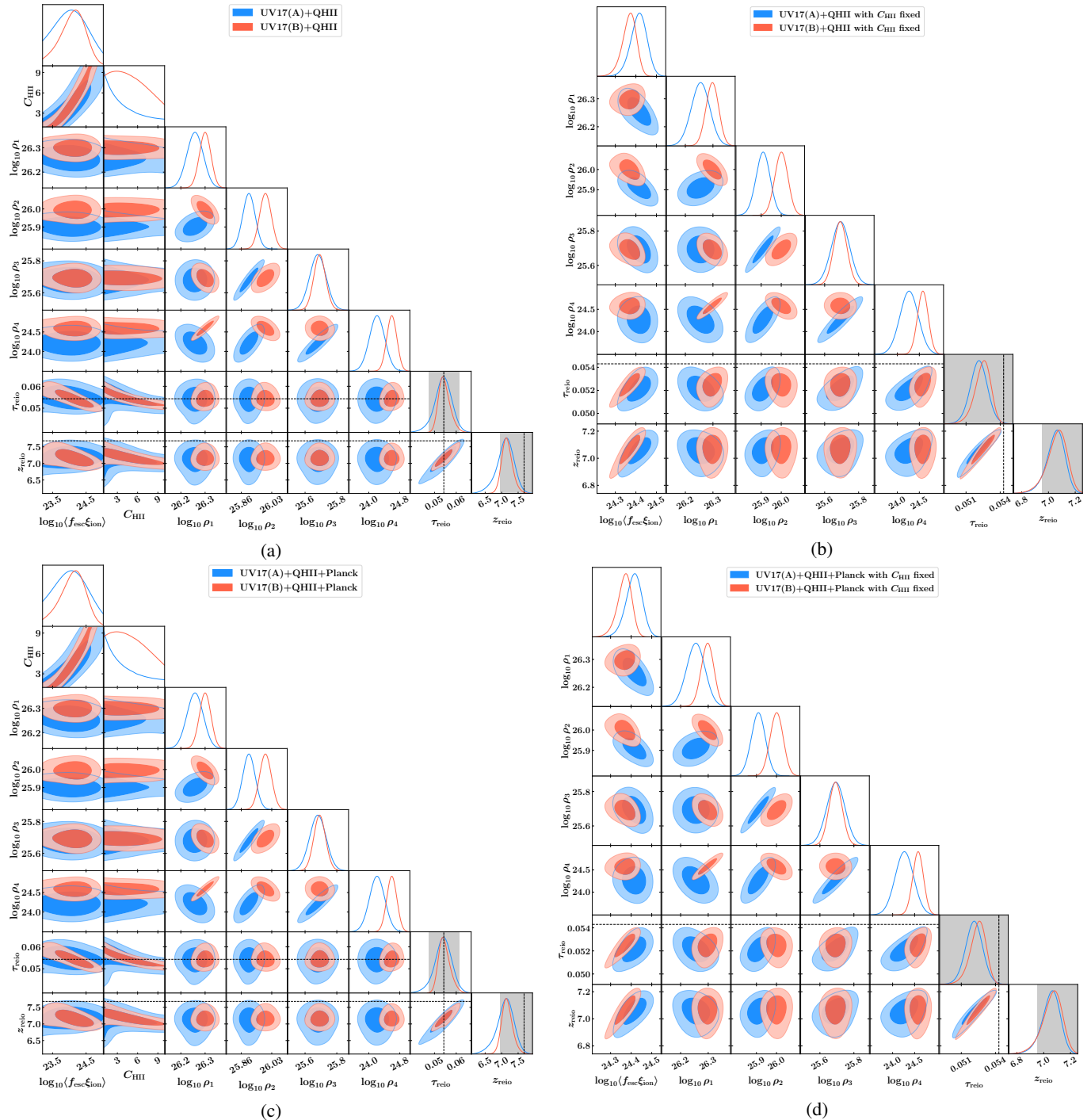


Figure 2. Comparison between the constraints obtained on the astrophysical parameters employing the (a) UV17(A)+QHII vs UV17(B)+QHII, (b) with the clumping factor kept constant at $C_{\text{HII}}=5$, (c) UV17(A)+QHII+Planck vs UV17(B)+QHII+Planck, and (d) with the clumping factor kept constant at $C_{\text{HII}}=5$, during the MCMC. The black dashed line and shaded region represent the Planck best-fit with 1σ CL.

data in the UV17(B) compilation narrows down the range of possible values. We also find that the nature of correlations between the parameters $\log_{10} \rho_{1-4}$ remains unchanged on fixing the value of C_{HII} (for comparison see panels (a) and (c) vs (b) and (d) of Fig. 2).

We are now in a position to reconstruct the reionization history profile with the help of these obtained bounds on the parameters $\log_{10} \langle f_{\text{esc}} \xi_{\text{ion}} \rangle$, C_{HII} , and $\log_{10} \rho_{1-4}$, and by deriving the evolution of the ionization fraction via Eq. (1). Fig. 3 demonstrates the comparison between the reconstructed Q_{HII} using two different data compilations - UV17(A)+QHII+Planck in panel (a) vs

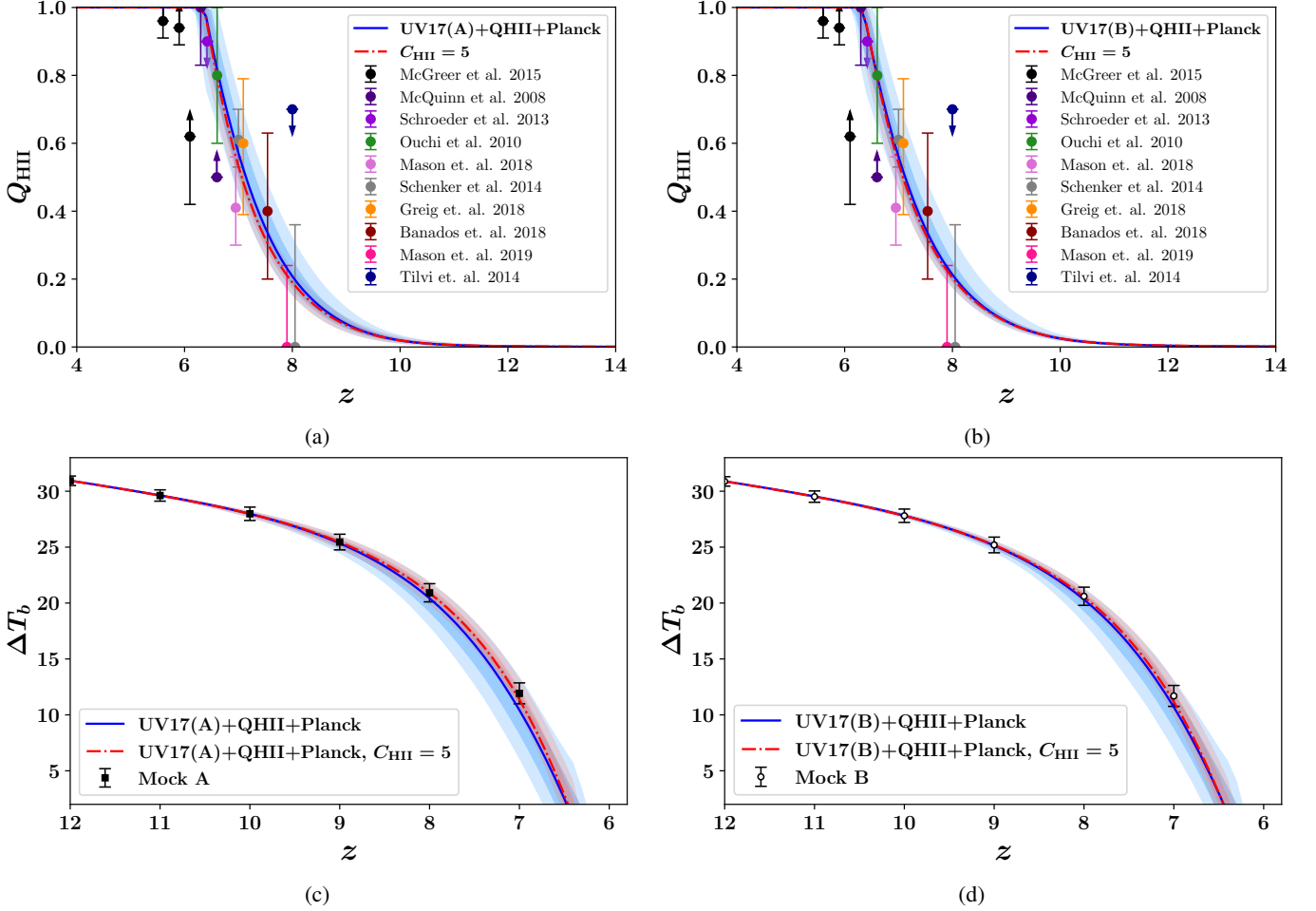


Figure 3. Evolution of the ionization fraction (Q_{HII}) and global 21-cm signal (ΔT_b) from reconstruction. Plots (a) and (b) show ionization fraction obtained using UV17+QHII+Planck (blue curve) vs UV17+QHII+Planck for a fixed value of the clumping factor $C_{\text{HII}} = 5$ (red dashed line) from the GP reconstruction of the UV luminosity density with the UV17(A) (left panels) and UV17(B) (right panels) compilation. Plots (c) and (d) show the global 21-cm signal at the reionization epoch from respective data sets. The QHII data is plotted with references for comparison. Mock A and B represent the simulated ΔT_b vs z catalogues.

UV17(B)+QHII+Planck in panel (b). With this reconstructed Q_{HII} profile, we can trace the nature of the 21-cm global brightness temperature fluctuation ΔT_b , directly employing Eq. (8). Plots for the reconstructed ΔT_b for the UV17(A)+QHII+Planck and UV17(B)+QHII+Planck data sets are shown in the panels (c) and (d) of Fig. 3 respectively. As depicted in Fig. 3, we obtain more or less similar results for the reionization history profile and global signal employing Planck+QHII+ either UV17(A) or UV17(B) data sets. Fixing the clumping factor C_{HII} to a constant value (here $C_{\text{HII}} = 5$) results in a more precise reconstruction of both Q_{HII} and ΔT_b . This feature is apparent from Fig. 2(b) and 2(d), where we notice a significant reduction of the $\langle f_{\text{esc}} \xi_{\text{ion}} \rangle$ parameter space obtained with MCMC analysis. However, one should take it with a pinch of salt, as there is no a priori reason as to why C_{HII} has to take a fixed value, especially when the parameters are not indifferent to a running C_{HII} and hence, the constraints obtained by keeping C_{HII} free should be more acceptable in a conservative approach.

6.2. Forecasting on upcoming surveys

Let us now engage ourselves in investigating the role of the global 21-cm signal on this reconstruction. After plotting the evolution of the 21-cm global signal with best-fit astrophysical parameters from UV17(A)+QHII+Planck and UV17(B)+QHII+Planck data, we create mock global 21-cm signal ΔT_b vs z data (shown in Fig. 3(c)-(d)), assuming the instrumental specifications of SARAS. We then redo this entire exercise of learning the reionization history incorporating the SARAS mock data in combination with the remaining UV17(A)/UV17(B), QHII and Planck data sets. Similar to the previous plots, Fig. 4(a)-(b) shows the 2D-confidence contours and 1D-marginalized posteriors for the MCMC parameter space using the joint UV17(A)+QHII+Planck+SARAS and UV17(B)+QHII+Planck+SARAS data sets, respectively. In panel (a) of Fig. 4, the clump-

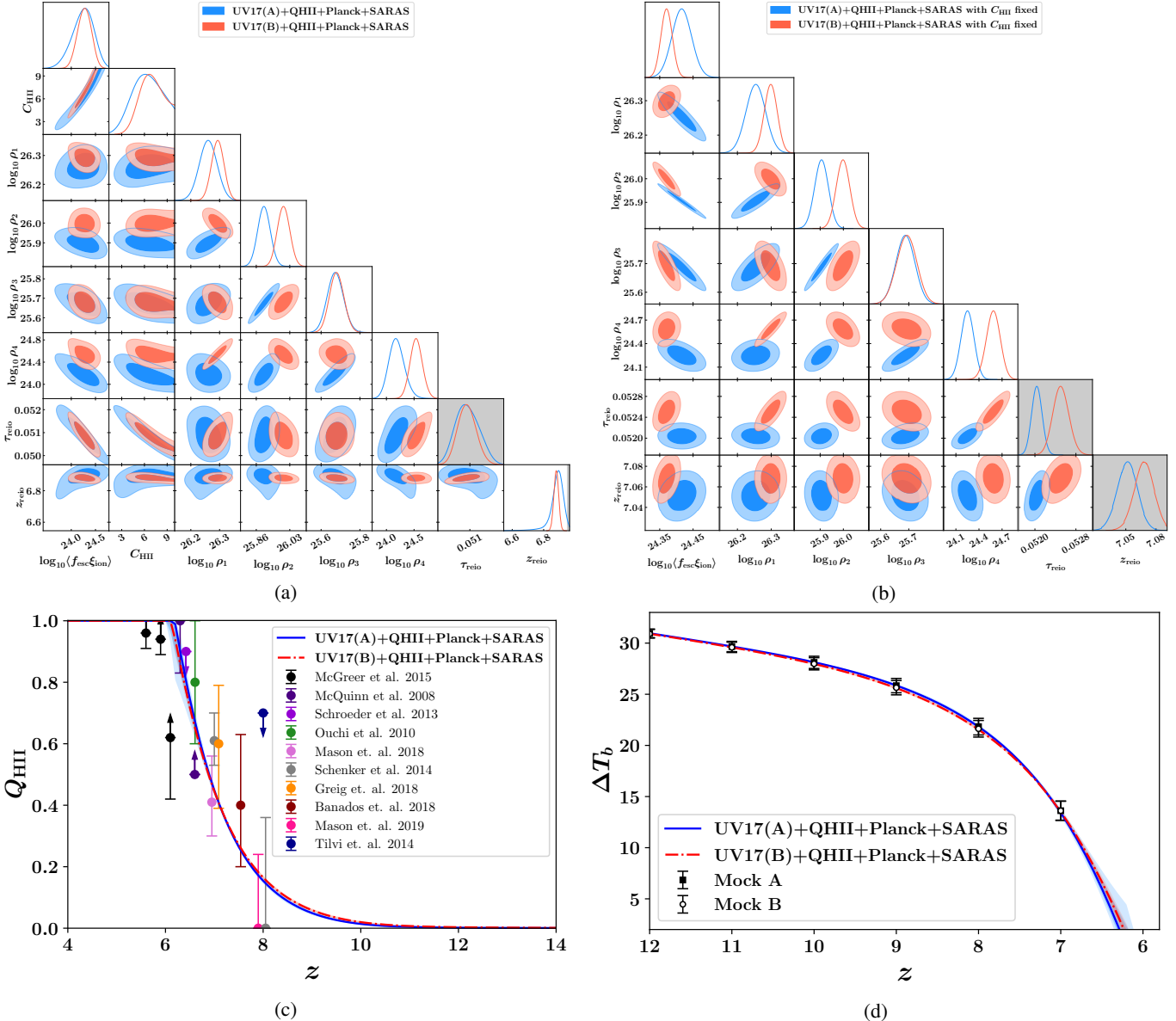


Figure 4. Comparison between the bounds obtained on the astrophysical parameters using UV17(A)+QHII+Planck+SARAS vs UV17(B)+QHII+Planck+SARAS and (b) with a constant clumping factor of $C_{\text{HII}} = 5$ (panel (b)). Evolution of the ionization fraction in (c) and the global 21-cm signal at reionization epoch in (d) obtained using UV17(A)+QHII+Planck+SARAS (blue curve) and UV17(B)+QHII+Planck+SARAS (red dashed line) from the GP reconstruction of the UV luminosity density with the UV17(A) and UV17(B) compilations respectively

ing factor C_{HII} is treated as a free parameter during MCMC, whereas, panel (b) shows the case when the value of the clumping factor is kept fixed at $C_{\text{HII}} = 5$ respectively. Therefore, the inclusion of SARAS data, as shown in Fig. 4, provides much tighter bounds on the astrophysical parameters. We also plot the evolution of the ionization fraction and global 21-cm signal at the reionization epoch, in the Fig. 4(c) and Fig. 4(d), respectively. Our findings show that the reconstructed Q_{HII} and ΔT_b profiles are now further constrained, compared to the previous cases. Thus, one can conclude that although the UV17(A)+QHII+Planck and UV17(B)+QHII+Planck data influence the reionization history and bounds on the astrophysical parameters, the global differential brightness temperature has a more significant impact on these parameters, thereby helping to learn the cosmic reionization history with better precision.

The constraints on the astrophysical parameters $\log_{10} \langle f_{\text{esc}} \xi_{\text{ion}} \rangle$, C_{HII} , optical depth τ_{reio} , reionization redshift z_{re} and reionization duration Δz , separately for each individual data compilations explored in the present analysis, are summarized in Table 1. The table shows that the optical depth constraints from all the combinations - UV17+QHII, UV17+QHII+Planck and

Data sets	$\log_{10}\langle f_{\text{esc}} \xi_{\text{ion}} \rangle$	C_{HII}	τ_{reio}	z_{reio}	Δz
UV17(A)+QHII	$24.001^{+0.405}_{-0.853}$	$3.302^{+3.648}_{-1.967}$	$0.054^{+0.0038}_{-0.0026}$	$7.12^{+0.21}_{-0.19}$	$2.21^{+1.23}_{-0.19}$
UV17(A)+QHII, $C_{\text{HII}} = 5$	$24.417^{+0.032}_{-0.039}$	5	$0.052^{+0.0007}_{-0.0007}$	$7.06^{+0.05}_{-0.07}$	$2.15^{+0.14}_{-0.12}$
UV17(A)+QHII+Planck	$24.192^{+0.281}_{-0.411}$	$4.582^{+3.197}_{-2.191}$	$0.054^{+0.0033}_{-0.0019}$	$7.13^{+0.19}_{-0.11}$	$2.17^{+0.24}_{-0.15}$
UV17(A)+QHII+Planck, $C_{\text{HII}} = 5$	$24.416^{+0.034}_{-0.040}$	5	$0.052^{+0.0007}_{-0.0007}$	$7.06^{+0.05}_{-0.07}$	$2.15^{+0.14}_{-0.13}$
UV17(A)+QHII+Planck+SARAS	$24.192^{+0.281}_{-0.411}$	$4.582^{+3.197}_{-2.191}$	$0.054^{+0.0033}_{-0.0019}$	$7.13^{+0.19}_{-0.11}$	$2.17^{+0.24}_{-0.15}$
UV17(A)+QHII+Planck+SARAS, $C_{\text{HII}} = 5$	$24.416^{+0.027}_{-0.028}$	5	$0.052^{+0.0001}_{-0.0001}$	$7.05^{+0.01}_{-0.01}$	$2.13^{+0.06}_{-0.05}$
UV17(B)+QHII	$24.164^{+0.262}_{-0.458}$	$4.760^{+2.978}_{-2.485}$	$0.054^{+0.0034}_{-0.0015}$	$7.13^{+0.18}_{-0.10}$	$2.25^{+0.20}_{-0.07}$
UV17(B)+QHII, $C_{\text{HII}} = 5$	$24.373^{+0.026}_{-0.037}$	5	$0.053^{+0.0005}_{-0.0007}$	$7.08^{+0.04}_{-0.09}$	$2.24^{+0.05}_{-0.04}$
UV17(B)+QHII+Planck	$24.200^{+0.247}_{-0.441}$	$5.081^{+3.027}_{-2.610}$	$0.054^{+0.0031}_{-0.0013}$	$7.12^{+0.17}_{-0.10}$	$2.25^{+0.15}_{-0.08}$
UV17(B)+QHII+Planck, $C_{\text{HII}} = 5$	$24.374^{+0.025}_{-0.036}$	5	$0.053^{+0.0005}_{-0.0007}$	$7.08^{+0.05}_{-0.08}$	$2.25^{+0.06}_{-0.05}$
UV17(B)+QHII+Planck+SARAS	$24.273^{+0.145}_{-0.141}$	$6.723^{+1.933}_{-1.304}$	$0.051^{+0.0004}_{-0.0004}$	$6.88^{+0.01}_{-0.01}$	$2.24^{+0.04}_{-0.03}$
UV17(B)+QHII+Planck+SARAS, $C_{\text{HII}} = 5$	$24.370^{+0.017}_{-0.016}$	5	$0.053^{+0.0001}_{-0.0001}$	$7.07^{+0.01}_{-0.01}$	$2.25^{+0.03}_{-0.04}$

Table 1. Summary of the mean and 1σ bounds obtained on the astrophysical parameters and reionization history using different data compilations.

UV17+QHII+Planck+SARAS align with the 1σ optical depth values from Planck 2018 results. Our analysis of reionization duration, Δz , suggests that a substantial portion of reionization (from 10% to 90% ionization) occurs over approximately 2 units (for Planck+UV17+QHII). The 68% and 95% confidence intervals reveal that the marginalized posterior distribution of Δz is slightly skewed when the clumping factor is free to vary during the MCMC. The redshift at which reionization reaches 50% completion, denoted as z_{reio} , is found to be approximately 7 for all the above-mentioned data combinations. The table shows that the mean value of $\log_{10}\langle f_{\text{esc}} \xi_{\text{ion}} \rangle$ parameter is approximately 24 units from all combinations of data sets. With the inclusion of SARAS data and keeping C_{HII} fixed, the 1σ bounds on the $\log_{10}\langle f_{\text{esc}} \xi_{\text{ion}} \rangle$ parameter are significantly constrained. The C_{HII} parameter takes different values for different data set combinations. The 1σ bound on this parameter improves with the UV17(B)+QHII+Planck+SARAS data set combination.

Our final target is to explore the prospects of the upcoming 21-cm mission SKA in simultaneously inferring the 2 astrophysical + 6 cosmological parameters. For this, we make use of the reconstructed reionization history and compute the 21-cm power spectrum during the reionization epoch with a conservative approach, employing Eq. (10). Further, we modify the Boltzmann solver code CLASS in order to accommodate our reconstructed reionization history (as opposed to using baseline Planck tanh reionization model), as explained in Sec. 5.3. The underlying cosmological model was set to the standard 6-parameter Λ CDM framework. Following the prescription given by Sprenger et al. (2019), we generate mock catalogues for the future SKA mission in the reionization era between redshift $z \approx 6 - 12$, from the simulated Planck realistic data, utilizing the `fake_planck_realistic` likelihood in MontePython (hereafter referred to as Planck) and MIKE-HIRES Lyman- α forest dataset, adopting the fiducial values of the cosmological parameters as $w_b = 0.02237$, $w_{\text{cdm}} = 0.12010$, $\ln[10^{10} A_s] = 3.0447$, $n_s = 0.9659$, $H_0 = 67.8$ km Mpc $^{-1}$ s $^{-1}$, $\tau_{\text{reio}} = 0.0543$, consistent with Planck 2018 data (Planck Collaboration et al. 2020). Finally, we undertake a Bayesian MCMC analysis to forecast the 6 cosmological and 2 astrophysical parameters using the MontePython code. We adopt uniform priors for all parameters as: $100 \Omega_b h^2 \in \mathcal{U}[0.05, 10]$, $\Omega_c h^2 \in \mathcal{U}[0.01, 0.99]$, $H_0 \in \mathcal{U}[50, 100]$, $n_s \in \mathcal{U}[0.5, 1.5]$, $\tau_{\text{reio}} \in \mathcal{U}[0.004, 0.2]$, $\ln(10^{10} A_s) \in \mathcal{U}[1, 5]$, $\langle f_{\text{esc}} \xi_{\text{ion}} \rangle \in \mathcal{U}[20, 30]$, and $C_{\text{HII}} \leq 10$ respectively. The resulting 2D-confidence contours and 1D-marginalized posteriors for the Planck+SKA+Ly α +UV17(A) and Planck+SKA+Ly α +UV17(B) data sets have been presented in Fig. 5, which also helps us in easy comparison between the two data sets. Table 2 presents the mean and 1σ bound on the astrophysical and cosmological parameters obtained from this analysis. Besides, we also show the results for two derived parameters z_{reio} and $\sigma_{8,0}$.

A comparison of the results presented in Table 1 and Table 2 for the two key cosmological parameters τ_{reio} and z_{reio} , as well as the two astrophysical parameters C_{HII} and $\langle f_{\text{esc}} \xi_{\text{ion}} \rangle$ is in order. Based on the power spectrum analysis, we achieve tighter 1σ bounds on the astrophysical parameters $\log_{10}\langle f_{\text{esc}} \xi_{\text{ion}} \rangle$ and C_{HII} compared to the results in Table 1. The parameter z_{reio} , which denotes the redshift at which 50% ionization is complete, shows a relatively higher value from the power spectrum analysis (somewhat akin to tanh reionization model) than from the global signal reconstruction analysis. However, a crucial difference between the two analyses needs to be kept in mind. In the power spectrum analysis, we considered the full fake Planck realistic

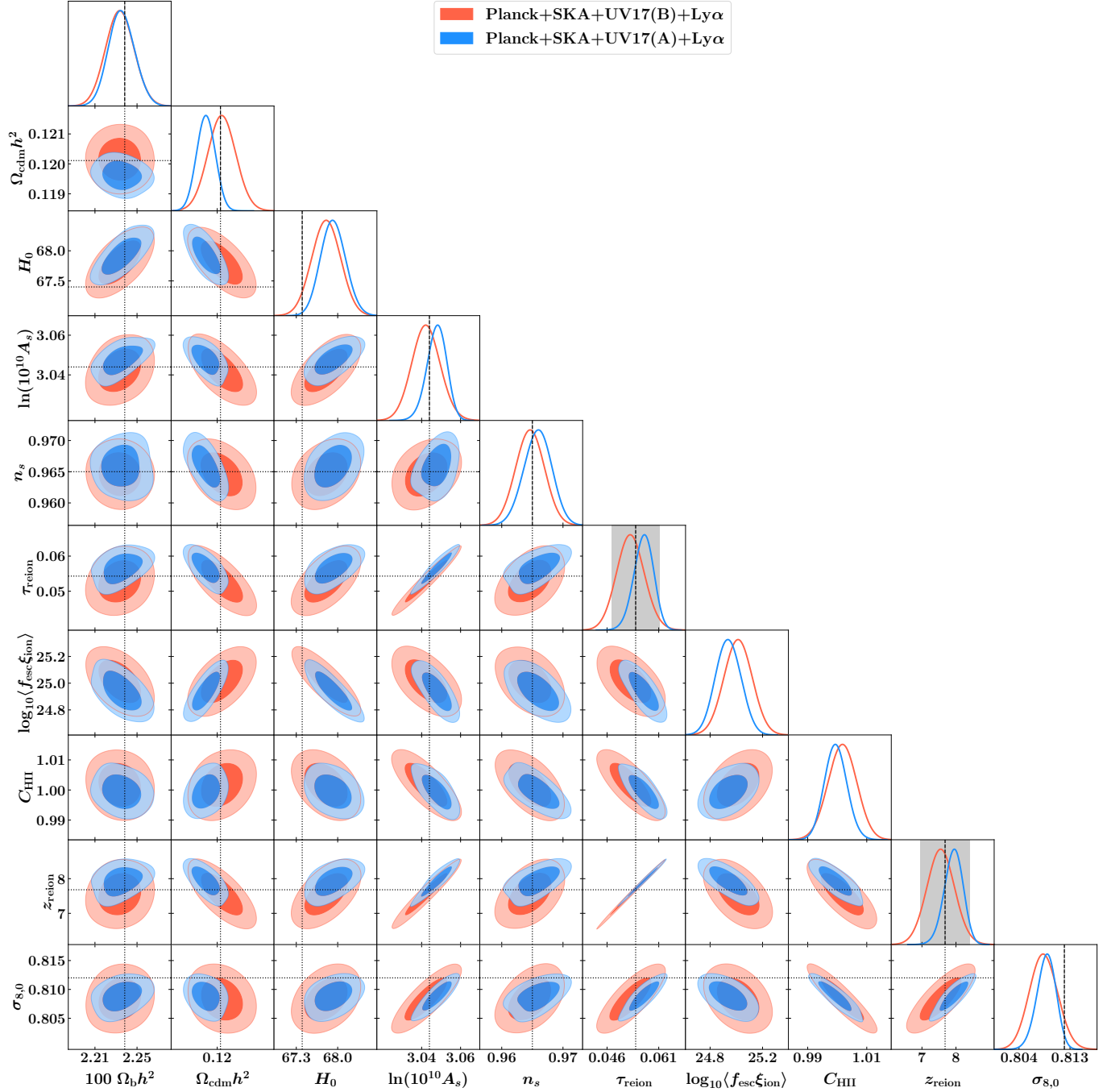


Figure 5. Forecasting the reionization power spectrum of 6 Λ CDM parameters with 2 astrophysical parameters: ionization efficiency and clumping factor, using the Planck+SKA+Ly α +UV17(A) data sets and the Planck+SKA+Ly α +UV17(B) data sets. Here for this forecast and MCMC analysis, we have used fake Planck realistic data. The analysis is undertaken using the mean reconstructed Q_{HII} function, without incorporating the errors.

data and ran MCMC for the 6 cosmological parameters along with the astrophysical parameters. In contrast, for the global signal reconstruction, we used the Planck optical depth measurement and ran MCMC for the astrophysical parameters only. This difference may have shown up as the slight difference in the z_{reio} values estimated from the two analyses and one should rely more on the “all parameters open” case than the other one.

Further, for comparison with the baseline reionization model, we also present the results for the 6-parameter Λ CDM with tanh reionization model in Table 2, which shows that our obtained values of τ_{reio} , z_{reio} , H_0 , σ_8 , and other cosmological parameters

Parameters	tanh reionization model ^a	GP reconstructed reionization model	
	Planck 2018 TT,TE,EE + lowE	Planck+SKA+Ly α +UV17(A)	Planck+SKA+Ly α +UV17(B)
$\log_{10}\langle f_{\text{esc}} \xi_{\text{ion}} \rangle$	23 – 500	$24.94^{+0.0095}_{-0.01}$	$24.95^{+0.093}_{-0.11}$
C_{HII}	1 – 10	$1.006^{+0.0059}_{-0.006}$	$1.003^{+0.0037}_{-0.003}$
$100 \Omega_b h^2$	2.236 ± 0.015	$2.235^{+0.0095}_{-0.013}$	$2.232^{+0.01}_{-0.013}$
$\Omega_{\text{cdm}} h^2$	0.1202 ± 0.0014	$0.1196^{+0.00033}_{-0.00031}$	$0.1197^{+0.0003}_{-0.0004}$
H_0	67.27 ± 0.60	$67.92^{+0.19}_{-0.21}$	$67.9^{+0.21}_{-0.22}$
$\ln(10^{10} A_s)$	3.045 ± 0.016	$3.047^{+0.0066}_{-0.0045}$	$3.045^{+0.0056}_{-0.0064}$
n_s	0.9649 ± 0.0044	$0.9658^{+0.0023}_{-0.0019}$	$0.9656^{+0.0024}_{-0.002}$
τ_{reio}	$0.0544^{+0.0070}_{-0.0081}$	$0.0566^{+0.003}_{-0.0025}$	$0.05595^{+0.0037}_{-0.0027}$
$100 \theta_s$	1.04077 ± 0.00047	$1.044^{+0.00027}_{-0.00024}$	$1.044^{+0.00027}_{-0.00029}$
z_{reio}	7.68 ± 0.79	$7.93^{+0.28}_{-0.26}$	$7.865^{+0.36}_{-0.26}$
σ_8	0.8120 ± 0.0073	$0.8088^{+0.0019}_{-0.0013}$	$0.8087^{+0.002}_{-0.0015}$

^a The values of the astrophysical parameters are taken from (Barkana & Loeb 2001; Mesinger et al. 2016; Price et al. 2016; Sarkar et al. 2016; Das et al. 2018; Dayal & Ferrara 2018; Dey et al. 2023a)

Table 2. Summary of the mean and 1σ bounds obtained on the astrophysical and cosmological parameters using the tanh model of reionization for Planck TT + lowE data (Planck Collaboration et al. 2020) and using the reconstructed reionization history for the Planck+SKA+Ly α +UV17(A) and UV17(B) data sets. Note that the allowed ranges of the two astrophysical parameters $\log_{10}\langle f_{\text{esc}} \xi_{\text{ion}} \rangle$, C_{HII} are derived from different astrophysical observations, without considering the tanh reionization model, while for the rest of the cosmological parameters, the allowed ranges are based on the tanh reionization model.

using the GP reconstructed reionization history are well consistent with the Planck 2018 + baseline model. On top of that, both of the astrophysical parameters C_{HII} and $\langle f_{\text{esc}} \xi_{\text{ion}} \rangle$ prefer values closer to the lower bounds of the tanh model. This happens in spite of choosing a wide prior range for both of them. We observe that the mean values of H_0 remain almost unaffected and lie close to the baseline Planck values, similar to Chatterjee et al. (2021). However, the mean value of σ_8 slightly decreases when changing the reionization history. This feature is similar to previous observations made in Fig. 4 of Hazra et al. (2020) using non-parametric nodal reconstruction, nonetheless that the astrophysical parameters were kept fixed to $\log_{10}\langle f_{\text{esc}} \xi_{\text{ion}} \rangle = 24.85$ (Ishigaki et al. 2015) and $C_{\text{HII}} \leq 3$, focusing on examining how the reconstructed model affects the constraints on the cosmological parameters. Paoletti et al. (2021) extended this exercise by varying the reionization astrophysical parameters simultaneously with the cosmological parameters using Planck+UV17+QHII data sets. The constraints obtained on the key parameters, such as $\log_{10}\langle f_{\text{esc}} \xi_{\text{ion}} \rangle$ and τ_{reio} in Table 3 & 4 of Paoletti et al. (2021) are consistent with our results, shown in Table 2. We believe the above consistency checks make the reconstruction technique a robust learning process and the inferences on the astrophysical parameters obtained therefrom are quite reliable that can be used for future analysis.

7. CONCLUDING REMARKS

In this article, we have investigated how GPR can enhance our understanding the history of reionization and associated astrophysical parameters during this period. We trained the GP algorithm for model-independent reconstruction of the UV luminosity function using UV17 data, which is then combined with the Planck optical depth and QHII Lyman- α measurements to undertake a non-parametric reconstruction of the reionization history. For a robust analysis, we allowed the parameters of the logarithmic double power law and kernel hyperparameters to vary freely during GP training, expanding upon previous literature (Ishigaki et al. 2018; Hazra et al. 2020; Adak et al. 2024), and found our results to be consistent. The clumping factor C_{HII} was kept free, rather than being fixed to specific values like 3 (Hazra et al. 2020) or 5 (Adak et al. 2024), allowing us to explore potential redshift variations and compare the roles of astrophysical parameters in shaping the reionization history.

We extended our analysis to explore previously unexplored applications of GPR in reionization. This involved separately considering the global 21-cm signal and the 21-cm power spectrum to investigate their roles in learning the astrophysical parameters and reionization history. For the global 21-cm signal, we trained GPR using SARAS mock data and found that its inclusion in the reconstruction pipeline significantly improves the bounds on the astrophysical parameters. We presented the 21-cm power spectrum analysis based on the reconstructed reionization history, by making modifications to the Boltzmann solver CLASS and MCMC code MontePython. Our findings indicate that the power spectrum analysis for the modified reionization history with

future SKA will help improve the bounds on six cosmological parameters and two astrophysical parameters. Additionally, both of the astrophysical parameters prefer values closer to the lower bounds of the baseline tanh reionization model.

For the SARAS-inclusive analysis, we rely on mock global signal data generated using the best-fit parameters from the SARAS and SKA-excluded runs (i.e., UV17+QHII+Planck). While the posterior in the SARAS-excluded run favored higher values of $C_{\text{HII}} \sim 3 - 4$, the SARAS mock itself was generated with a *fixed* $C_{\text{HII}} \sim 4 - 5$ in this range, along with the corresponding best-fit values for other parameter, such as $\log_{10}\langle f_{\text{esc}} \xi_{\text{ion}} \rangle \sim 24.1 - 24.4$, respectively. Consequently, in the SARAS-inclusive analysis Fig. 4(a), the posterior naturally peaks tightly around $C_{\text{HII}} \sim 3 - 4$, reflecting the mock input bias rather than a rejection of lower values from real data. In the SKA-based analysis, mock power spectra are generated within the `MontePython` pipeline using the Planck 2018 cosmology and the GP-reconstructed reionization history (Table 1). Although the reconstruction accounts for the redshift evolution of the ionization fraction, the astrophysical parameters (e.g., $\log_{10}\langle f_{\text{esc}} \xi_{\text{ion}} \rangle$ and C_{HII}) are effectively averaged over redshift. From the power spectrum analysis with Planck+SKA+Ly α +UV17 data we found the 1σ bound on $C_{\text{HII}} \sim 1$.

Previous studies discuss the possibility of a wide range of C_{HII} values: hydrodynamical simulations of the early universe suggested $C_{\text{HII}} \sim 30$ (e.g. [Gnedin & Ostriker 1997](#)), implying that recombination played a significant role in the progression of reionization. Later dark-matter-only simulations yielded $C_{\text{HII}} \sim 10$ ([Iliev et al. 2005, 2007](#)), while radiation-hydrodynamic studies indicate lower values of 2–3 ([McQuinn et al. 2011](#)), though recent work points to somewhat higher estimates (e.g. [Kannan et al. 2022](#)). A redshift-dependent model, $C_{\text{HII}} = 2.9 \times \left(\frac{1+z}{2}\right)^{-1.1}$ ([Paoletti et al. 2024; Shull et al. 2011](#)), suggests that low values (near unity) inferred from power spectrum-based mocks are consistent with early reionization, while higher values from global-signal mocks reflect later stages.

Again, while f_{esc} is particularly difficult to constrain at $z \sim 2 - 4.5$ ([Inoue et al. 2014; Robertson 2021](#)), early studies favored low values ($f_{\text{esc}} \approx 0.2$) consistent with CMB and HFF data ([Robertson et al. 2013](#)). More recent JWST results indicate higher ξ_{ion} at $z > 9$, highlighting a degeneracy between ξ_{ion} and f_{esc} ([Muñoz et al. 2024; Simmonds et al. 2024; Atek et al. 2024](#)). Studies also suggest f_{esc} evolves with redshift ([Kulkarni et al. 2019; Finkelstein et al. 2019; Cain et al. 2021; Katz et al. 2023](#)), though a constant $f_{\text{esc}} \sim 0.06 - 0.1$ for $z \geq 6$ is consistent with current data ([Mitra & Chatterjee 2023](#)). Within ΛCDM , the product $\xi_{\text{ion}} f_{\text{esc}}$ varies widely across reionization models, complicating cosmological interpretations ([Hazra et al. 2020; Paoletti et al. 2021; Chatterjee et al. 2021; Dey et al. 2023a,b; Paoletti et al. 2024](#)). Our results for $\log_{10}\langle f_{\text{esc}} \xi_{\text{ion}} \rangle$ and z_{reio} agree well with existing constraints.

However, it is important to emphasize that the constraints derived from SARAS and SKA mock analyses are dependent on underlying mock datasets. To investigate this difference in the resulting C_{HII} constraints between the SARAS- vs SKA-inclusive analyses, we further regenerated the SARAS mock with $C_{\text{HII}} \sim 1$ and a lower input value of $\log_{10}\langle f_{\text{esc}} \xi_{\text{ion}} \rangle \sim 23.2 - 23.4$. In this case, we recover $C_{\text{HII}} \sim 1$ as an allowed value, but observe a significant shift in $\log_{10}\langle f_{\text{esc}} \xi_{\text{ion}} \rangle$. This again confirms a strong degeneracy between C_{HII} and $\log_{10}\langle f_{\text{esc}} \xi_{\text{ion}} \rangle$. Therefore, when fitting the mock SARAS data, the posterior for C_{HII} peaks sharply around the injected value not due to rejection of other values from actual data, but because the mock input enforces this value, maintaining the corelation with $\log_{10}\langle f_{\text{esc}} \xi_{\text{ion}} \rangle$.

As a result, the apparent variation in C_{HII} and $\log_{10}\langle f_{\text{esc}} \xi_{\text{ion}} \rangle$ across SARAS- and SKA-inclusive analyses primarily reflects their differing redshift sensitivities. Any true underlying redshift evolution in $C_{\text{HII}}(z)$ or $\log_{10}\langle f_{\text{esc}} \xi_{\text{ion}} \rangle$, which is not explicitly modeled in this work, would naturally lead to different recovered values in the SARAS and SKA analyses pipelines, without implying a contradiction. Furthermore, we would like to clarify that the recovered parameter values are reflective of different effective redshift regimes, and should not be compared without accounting for potential redshift evolution. This underscores our main conclusion: both global signal (e.g. SARAS) and power spectrum (e.g. SKA) probes offer complementary insight into EoR astrophysics, and future datasets will be key in breaking degeneracies between the astrophysical parameters.

Thus, differences in C_{HII} from SKA- vs. SARAS-based analyses reflect redshift evolution rather than inconsistency. Our goal here is not to assert statistical consistency or tension between the values of C_{HII} across analyses, but rather to emphasize the complementary nature of the information the global signal or power spectrum can provide. The global signal and power spectrum analyses are two important and distinct types of observables in 21 cm cosmology. In global signal analysis, only the spatially averaged (global) quantities are considered, without accounting for perturbations. In contrast, power spectrum analysis explicitly includes the spatial fluctuations of different components. As a result, these two analyses probe different aspects of the 21 cm signal and are fundamentally different in nature. Thus in this paper two analysis gives the complete pictures of the reionization history of the Universe. As our analysis is based on idealized mock datasets, we refrain from making strong statistical claims at this stage.

Thus, our analysis demonstrates that GPR-based reconstruction performs well in the context of reionization, both for the global 21-cm signal and the 21-cm power spectrum, in combination with other relevant data sets. The results derived from our method are hence reliable and can be used in future reionization studies. That said, our reconstruction framework can be extended in

several directions. The current power spectrum analysis is based on Eq. (10) and does not yet include the redshift evolution of $\log_{10}\langle f_{\text{esc}} \xi_{\text{ion}} \rangle$, though we do incorporate redshift evolution in C_{HII} . A more rigorous analysis will involve reionization simulation for estimating the actual bounds on the astrophysical parameters and possible reflections on SKA (Mangena et al. 2020). Further, our analysis is based only on the Λ CDM model; as our future goal, we will explore beyond- Λ CDM models and investigate their impact on the reionization period.

For reconstruction purposes, the kinetic Sunyaev-Zeldovich data (Jain et al. 2024) can also be added on top of current data sets and the possible consequences can be investigated. Lastly, while we have utilized the GPR technique as an ML tool for learning, future investigations will explore various ML techniques (Sohn et al. 2024; Gómez-Vargas et al. 2023; Shah et al. 2024; Mukherjee et al. 2024a) for training and testing in the context of reionization. We look forward to pursuing these avenues in future work.

Software: emcee (Foreman-Mackey et al. 2013), CLASS (Blas et al. 2011), MontePython (Audren et al. 2013; Brinckmann & Lesgourgues 2019), GetDist (Lewis 2019)

1 We acknowledge Rahul Shah and Debarun Paul for their useful comments. PM would like to thank Dhiraj Kumar Hazra and
2 Anjan Ananda Sen for discussions. PM acknowledges funding from the Anusandhan National Research Foundation (ANRF),
3 Govt of India under the National Post-Doctoral Fellowship (File no. PDF/2023/001986). AD thanks IOP, Bhubaneswar for
4 financial support. SP thanks the Department of Science and Technology, Govt. of India for partial support through Grant No.
5 NMICPS/006/MD/2020-21 and also the ANRF, Govt. of India for partial support through Project No. CRG/2023/003984. The
6 authors gratefully acknowledge the computational facility of ISI Kolkata and the use of the High-Performance Computing facility,
7 Pegasus, at IUCAA, Pune, India.

REFERENCES

Abdurashidova, Z., et al. 2022, *Astrophys. J.*, 924, 51, doi: [10.3847/1538-4357/ac2ffc](https://doi.org/10.3847/1538-4357/ac2ffc)

Adak, D., Hazra, D. K., Mitra, S., & Krishak, A. 2024. <https://arxiv.org/abs/2405.10180>

Atek, H., Labb  , I., Furtak, L. J., et al. 2024, *Nature*, 626, 975, doi: [10.1038/s41586-024-07043-6](https://doi.org/10.1038/s41586-024-07043-6)

Audren, B., Lesgourgues, J., Benabed, K., & Prunet, S. 2013, *JCAP*, 1302, 001, doi: [10.1088/1475-7516/2013/02/001](https://doi.org/10.1088/1475-7516/2013/02/001)

Barkana, R., & Loeb, A. 2001, *Phys. Rept.*, 349, 125, doi: [10.1016/S0370-1573\(01\)00019-9](https://doi.org/10.1016/S0370-1573(01)00019-9)

Blas, D., Lesgourgues, J., & Tram, T. 2011, *JCAP*, 07, 034, doi: [10.1088/1475-7516/2011/07/034](https://doi.org/10.1088/1475-7516/2011/07/034)

Bolton, J. S., Haehnelt, M. G., Warren, S. J., et al. 2011, *MNRAS*, 416, L70, doi: [10.1111/j.1745-3933.2011.01100.x](https://doi.org/10.1111/j.1745-3933.2011.01100.x)

Bouwens, R., Illingworth, G., Oesch, P., et al. 2023, *Mon. Not. Roy. Astron. Soc.*, 523, 1009, doi: [10.1093/mnras/stad1014](https://doi.org/10.1093/mnras/stad1014)

Bouwens, R. J., Illingworth, G. D., Oesch, P. A., et al. 2015a, *Astrophys. J.*, 811, 140, doi: [10.1088/0004-637X/811/2/140](https://doi.org/10.1088/0004-637X/811/2/140)

Bouwens, R. J., Oesch, P. A., Illingworth, G. D., Ellis, R. S., & Stefanon, M. 2017, *Astrophys. J.*, 843, 129, doi: [10.3847/1538-4357/aa70a4](https://doi.org/10.3847/1538-4357/aa70a4)

Bouwens, R. J., et al. 2015b, *Astrophys. J.*, 803, 34, doi: [10.1088/0004-637X/803/1/34](https://doi.org/10.1088/0004-637X/803/1/34)

Bouwens, R. J., Oesch, P. A., Stefanon, M., et al. 2021, *AJ*, 162, 47, doi: [10.3847/1538-3881/abf83e](https://doi.org/10.3847/1538-3881/abf83e)

Brinckmann, T., & Lesgourgues, J. 2019, *Phys. Dark Univ.*, 24, 100260, doi: [10.1016/j.dark.2018.100260](https://doi.org/10.1016/j.dark.2018.100260)

Cain, C., D'Aloisio, A., Gangolli, N., & Becker, G. D. 2021, *ApJL*, 917, L37, doi: [10.3847/2041-8213/ac1ace](https://doi.org/10.3847/2041-8213/ac1ace)

Chatterjee, A., Choudhury, T. R., & Mitra, S. 2021, *Mon. Not. Roy. Astron. Soc.*, 507, 2405, doi: [10.1093/mnras/stab2316](https://doi.org/10.1093/mnras/stab2316)

Choudhury, T. R. 2009, *Current Science*, 97, 841, doi: [10.48550/arXiv.0904.4596](https://doi.org/10.48550/arXiv.0904.4596)

Choudhury, T. R., & Ferrara, A. 2005, *Mon. Not. Roy. Astron. Soc.*, 361, 577, doi: [10.1111/j.1365-2966.2005.09196.x](https://doi.org/10.1111/j.1365-2966.2005.09196.x)

Das, S., Mondal, R., Rentala, V., & Suresh, S. 2018, *JCAP*, 2018, 045, doi: [10.1088/1475-7516/2018/08/045](https://doi.org/10.1088/1475-7516/2018/08/045)

Davies, F. B., et al. 2018, *Astrophys. J.*, 864, 142, doi: [10.3847/1538-4357/aad6dc](https://doi.org/10.3847/1538-4357/aad6dc)

Dayal, P., & Ferrara, A. 2018, *Phys. Rept.*, 780-782, 1, doi: [10.1016/j.physrep.2018.10.002](https://doi.org/10.1016/j.physrep.2018.10.002)

de Lera Acedo, E., Razavi-Ghods, N., Troop, N., Drought, N., & Faulkner, A. J. 2015, *Experimental Astronomy*, 39, 567, doi: [10.1007/s10686-015-9439-0](https://doi.org/10.1007/s10686-015-9439-0)

de Oliveira-Costa, A., Tegmark, M., Gaensler, B. M., et al. 2008, *Mon. Not. Roy. Astron. Soc.*, 388, 247, doi: [10.1111/j.1365-2966.2008.13376.x](https://doi.org/10.1111/j.1365-2966.2008.13376.x)

Dewdney, P. E., & Braun, R. 2016, *SKA Organisation*, 2, 1

Dey, A., Paul, A., & Pal, S. 2023a, *Mon. Not. Roy. Astron. Soc.*, 524, 100, doi: [10.1093/mnras/stad1838](https://doi.org/10.1093/mnras/stad1838)

—. 2023b, *Mon. Not. Roy. Astron. Soc.*, 527, 790, doi: [10.1093/mnras/stad3180](https://doi.org/10.1093/mnras/stad3180)

Ellis, R. S., et al. 2013, *Astrophys. J. Lett.*, 763, L7, doi: [10.1088/2041-8205/763/1/L7](https://doi.org/10.1088/2041-8205/763/1/L7)

Finkelstein, S. L., D'Aloisio, A., Paardekooper, J.-P., et al. 2019, *ApJ*, 879, 36, doi: [10.3847/1538-4357/ab1ea8](https://doi.org/10.3847/1538-4357/ab1ea8)

Finlator, K., Oh, S. P., Ozel, F., & Dave, R. 2012, *Mon. Not. Roy. Astron. Soc.*, 427, 2464, doi: [10.1111/j.1365-2966.2012.22114.x](https://doi.org/10.1111/j.1365-2966.2012.22114.x)

Foreman-Mackey, D., Hogg, D. W., Lang, D., & Goodman, J. 2013, *Publ. Astron. Soc. Pac.*, 125, 306, doi: [10.1086/670067](https://doi.org/10.1086/670067)

Furlanetto, S., Oh, S. P., & Briggs, F. 2006, *Phys. Rept.*, 433, 181, doi: [10.1016/j.physrep.2006.08.002](https://doi.org/10.1016/j.physrep.2006.08.002)

Gerardi, F., Martinelli, M., & Silvestri, A. 2019, *JCAP*, 07, 042, doi: [10.1088/1475-7516/2019/07/042](https://doi.org/10.1088/1475-7516/2019/07/042)

Gnedin, N. Y., & Ostriker, J. P. 1997, *Astrophys. J.*, 486, 581, doi: [10.1086/304548](https://doi.org/10.1086/304548)

Gómez-Vargas, I., Andrade, J. B., & Vázquez, J. A. 2023, *Phys. Rev. D*, 107, 043509, doi: [10.1103/PhysRevD.107.043509](https://doi.org/10.1103/PhysRevD.107.043509)

Gorce, A., Douspis, M., Aghanim, N., & Langer, M. 2018, *Astron. Astrophys.*, 616, A113, doi: [10.1051/0004-6361/201629661](https://doi.org/10.1051/0004-6361/201629661)

Greig, B., Mesinger, A., Haiman, Z., & Simcoe, R. A. 2017, *Mon. Not. Roy. Astron. Soc.*, 466, 4239, doi: [10.1093/mnras/stw3351](https://doi.org/10.1093/mnras/stw3351)

Harezlak, J., Ruppert, D., & Wand, M. P. 2018, *Semiparametric Regression with R* (New York: Springer)

Harikane, Y., Ono, Y., Ouchi, M., et al. 2022, *ApJS*, 259, 20, doi: [10.3847/1538-4365/ac3dfc](https://doi.org/10.3847/1538-4365/ac3dfc)

Harikane, Y., Ouchi, M., Oguri, M., et al. 2023, *ApJS*, 265, 5, doi: [10.3847/1538-4365/acaaa9](https://doi.org/10.3847/1538-4365/acaaa9)

Hazra, D. K., Paoletti, D., Finelli, F., & Smoot, G. F. 2020, *Phys. Rev. Lett.*, 125, 071301, doi: [10.1103/PhysRevLett.125.071301](https://doi.org/10.1103/PhysRevLett.125.071301)

Hirata, C. M. 2006, *Mon. Not. Roy. Astron. Soc.*, 367, 259, doi: [10.1111/j.1365-2966.2005.09949.x](https://doi.org/10.1111/j.1365-2966.2005.09949.x)

Iliev, I. T., Mellema, G., Pen, U.-L., et al. 2006, *Mon. Not. Roy. Astron. Soc.*, 369, 1625, doi: [10.1111/j.1365-2966.2006.10502.x](https://doi.org/10.1111/j.1365-2966.2006.10502.x)

Iliev, I. T., Mellema, G., Shapiro, P. R., & Pen, U.-L. 2007, *Mon. Not. Roy. Astron. Soc.*, 376, 534, doi: [10.1111/j.1365-2966.2007.11482.x](https://doi.org/10.1111/j.1365-2966.2007.11482.x)

Iliev, I. T., Scannapieco, E., & Shapiro, P. R. 2005, *Astrophys. J.*, 624, 491, doi: [10.1086/429083](https://doi.org/10.1086/429083)

Inoue, A. K., Shimizu, I., & Iwata, I. 2014, *Mon. Not. Roy. Astron. Soc.*, 442, 1805, doi: [10.1093/mnras/stu936](https://doi.org/10.1093/mnras/stu936)

Ishigaki, M., Kawamata, R., Ouchi, M., et al. 2015, *ApJ*, 799, 12, doi: [10.1088/0004-637X/799/1/12](https://doi.org/10.1088/0004-637X/799/1/12)

—. 2018, *ApJ*, 854, 73, doi: [10.3847/1538-4357/aaa544](https://doi.org/10.3847/1538-4357/aaa544)

Jain, D., Choudhury, T. R., Raghunathan, S., & Mukherjee, S. 2024, *Mon. Not. Roy. Astron. Soc.*, 530, 35, doi: [10.1093/mnras/stae748](https://doi.org/10.1093/mnras/stae748)

Kannan, R., Garaldi, E., Smith, A., et al. 2022, *Mon. Not. Roy. Astron. Soc.*, 511, 4005, doi: [10.1093/mnras/stab3710](https://doi.org/10.1093/mnras/stab3710)

Katz, H., et al. 2023, *Mon. Not. Roy. Astron. Soc.*, 518, 270, doi: [10.1093/mnras/stac3019](https://doi.org/10.1093/mnras/stac3019)

Krishak, A., & Hazra, D. K. 2021, *Astrophys. J.*, 922, 95, doi: [10.3847/1538-4357/ac3251](https://doi.org/10.3847/1538-4357/ac3251)

Kuhlen, M., & Faucher-Giguere, C. A. 2012, *Mon. Not. Roy. Astron. Soc.*, 423, 862, doi: [10.1111/j.1365-2966.2012.20924.x](https://doi.org/10.1111/j.1365-2966.2012.20924.x)

Kulkarni, G., Keating, L. C., Haehnelt, M. G., et al. 2019, *MNRAS*, 485, L24, doi: [10.1093/mnrasl/slz025](https://doi.org/10.1093/mnrasl/slz025)

Lewis, A. 2019. <https://arxiv.org/abs/1910.13970>

Lotz, J. M., et al. 2017, *Astrophys. J.*, 837, 97, doi: [10.17909/T9KK5N](https://doi.org/10.17909/T9KK5N)

Lotz, J. M., Koekemoer, A., Coe, D., et al. 2017, *ApJ*, 837, 97, doi: [10.3847/1538-4357/837/1/97](https://doi.org/10.3847/1538-4357/837/1/97)

Madau, P., Haardt, F., & Rees, M. J. 1999, *ApJ*, 514, 648, doi: [10.1086/306975](https://doi.org/10.1086/306975)

Madau, P., Meiksin, A., & Rees, M. J. 1997, *Astrophys. J.*, 475, 429, doi: [10.1086/303549](https://doi.org/10.1086/303549)

Mangena, T., Hassan, S., & Santos, M. G. 2020, *Mon. Not. Roy. Astron. Soc.*, 494, 600, doi: [10.1093/mnras/staa750](https://doi.org/10.1093/mnras/staa750)

Mason, C. A., Fontana, A., Treu, T., et al. 2019, *MNRAS*, 485, 3947, doi: [10.1093/mnras/stz632](https://doi.org/10.1093/mnras/stz632)

McGreer, I. D., Mesinger, A., & D'Odorico, V. 2015, *MNRAS*, 447, 499, doi: [10.1093/mnras/stu2449](https://doi.org/10.1093/mnras/stu2449)

McLeod, D. J., McLure, R. J., & Dunlop, J. S. 2016, *MNRAS*, 459, 3812, doi: [10.1093/mnras/stw904](https://doi.org/10.1093/mnras/stw904)

McLure, R. J., et al. 2013, *Mon. Not. Roy. Astron. Soc.*, 432, 2696, doi: [10.1093/mnras/stt627](https://doi.org/10.1093/mnras/stt627)

McQuinn, M., Lidz, A., Zaldarriaga, M., Hernquist, L., & Dutta, S. 2008, *MNRAS*, 388, 1101, doi: [10.1111/j.1365-2966.2008.13271.x](https://doi.org/10.1111/j.1365-2966.2008.13271.x)

McQuinn, M., Peng Oh, S., & Faucher-Giguère, C.-A. 2011, *The Astrophysical Journal*, 743, 82, doi: [10.1088/0004-637x/743/1/82](https://doi.org/10.1088/0004-637x/743/1/82)

Mesinger, A., Greig, B., & Sobacchi, E. 2016, *Mon. Not. Roy. Astron. Soc.*, 459, 2342, doi: [10.1093/mnras/stw831](https://doi.org/10.1093/mnras/stw831)

Mitra, S., & Chatterjee, A. 2023, *Mon. Not. Roy. Astron. Soc.*, 523, L35, doi: [10.1093/mnrasl/slad055](https://doi.org/10.1093/mnrasl/slad055)

Morandi, A., & Barkana, R. 2012, *MNRAS*, 424, 2551, doi: [10.1111/j.1365-2966.2012.21240.x](https://doi.org/10.1111/j.1365-2966.2012.21240.x)

Mortlock, D. J., Warren, S. J., Venemans, B. P., et al. 2011, *Nature*, 474, 616, doi: [10.1038/nature10159](https://doi.org/10.1038/nature10159)

Muñoz, J. B., Kovetz, E. D., Raccanelli, A., Kamionkowski, M., & Silk, J. 2017, *JCAP*, 05, 032, doi: [10.1088/1475-7516/2017/05/032](https://doi.org/10.1088/1475-7516/2017/05/032)

Muñoz, J. B., Mirocha, J., Chisholm, J., Furlanetto, S. R., & Mason, C. 2024. <https://arxiv.org/abs/2404.07250>

Mukherjee, P. 2022, PhD thesis, IISER, Kolkata. <https://arxiv.org/abs/2207.07857>

Mukherjee, P., Dialetopoulou, K. F., Levi Said, J., & Mifsud, J. 2024a. <https://arxiv.org/abs/2402.10502>

Mukherjee, P., Shah, R., Bhaumik, A., & Pal, S. 2024b, *Astrophys. J.*, 960, 61, doi: [10.3847/1538-4357/ad055f](https://doi.org/10.3847/1538-4357/ad055f)

Oesch, P. A., Bouwens, R. J., Illingworth, G. D., Labb  , I., & Stefanon, M. 2018, *ApJ*, 855, 105, doi: [10.3847/1538-4357/aab03f](https://doi.org/10.3847/1538-4357/aab03f)

Ono, Y., Ouchi, M., Mobasher, B., et al. 2012, *ApJ*, 744, 83, doi: [10.1088/0004-637X/744/2/83](https://doi.org/10.1088/0004-637X/744/2/83)

Paoletti, D., Hazra, D. K., Finelli, F., & Smoot, G. F. 2021, *Phys. Rev. D*, 104, 123549, doi: [10.1103/PhysRevD.104.123549](https://doi.org/10.1103/PhysRevD.104.123549)

—. 2024. <https://arxiv.org/abs/2405.09506>

Patra, N., Subrahmanyam, R., Raghunathan, A., & Udaya Shankar, N. 2013, *Experimental Astronomy*, 36, 319, doi: [10.1007/s10686-013-9336-3](https://doi.org/10.1007/s10686-013-9336-3)

Pawlak, A. H., Schaye, J., & van Scherpenzeel, E. 2009, *Mon. Not. Roy. Astron. Soc.*, 394, 1812, doi: [10.1111/j.1365-2966.2009.14486.x](https://doi.org/10.1111/j.1365-2966.2009.14486.x)

Planck Collaboration, Aghanim, N., Akrami, Y., et al. 2020, *A&A*, 641, A6, doi: [10.1051/0004-6361/201833910](https://doi.org/10.1051/0004-6361/201833910)

Price, L. C., Trac, H., & Cen, R. 2016. <https://arxiv.org/abs/1605.03970>

Pritchard, J. R., & Loeb, A. 2012, *Rept. Prog. Phys.*, 75, 086901, doi: [10.1088/0034-4885/75/8/086901](https://doi.org/10.1088/0034-4885/75/8/086901)

Rasmussen, C. E., & Williams, C. K. I. 2006, *Gaussian Processes for Machine Learning* (The MIT Press)

Robertson, B. E. 2021, *Annual Review of Astronomy and Astrophysics*, doi: [10.1146/annurev-astro-120221-044656](https://doi.org/10.1146/annurev-astro-120221-044656)

Robertson, B. E., et al. 2013, *Astrophys. J.*, 768, 71, doi: [10.1088/0004-637X/768/1/71](https://doi.org/10.1088/0004-637X/768/1/71)

Sarkar, A., Mondal, R., Das, S., et al. 2016, *JCAP*, 04, 012, doi: [10.1088/1475-7516/2016/04/012](https://doi.org/10.1088/1475-7516/2016/04/012)

Schechter, P. 1976, *Astrophys. J.*, 203, 297, doi: [10.1086/154079](https://doi.org/10.1086/154079)

Schenker, M. A., Ellis, R. S., Konidaris, N. P., & Stark, D. P. 2014, *ApJ*, 795, 20, doi: [10.1088/0004-637X/795/1/20](https://doi.org/10.1088/0004-637X/795/1/20)

Schenker, M. A., et al. 2013, *Astrophys. J.*, 768, 196, doi: [10.1088/0004-637X/768/2/196](https://doi.org/10.1088/0004-637X/768/2/196)

Schroeder, J., Mesinger, A., & Haiman, Z. 2013, *Mon. Not. Roy. Astron. Soc.*, 428, 3058, doi: [10.1093/mnras/sts253](https://doi.org/10.1093/mnras/sts253)

Seikel, M., Clarkson, C., & Smith, M. 2012, *JCAP*, 06, 036, doi: [10.1088/1475-7516/2012/06/036](https://doi.org/10.1088/1475-7516/2012/06/036)

Shafieloo, A., Kim, A. G., & Linder, E. V. 2012, *Phys. Rev. D*, 85, 123530, doi: [10.1103/PhysRevD.85.123530](https://doi.org/10.1103/PhysRevD.85.123530)

Shah, R., Bhaumik, A., Mukherjee, P., & Pal, S. 2023, *JCAP*, 06, 038, doi: [10.1088/1475-7516/2023/06/038](https://doi.org/10.1088/1475-7516/2023/06/038)

Shah, R., Saha, S., Mukherjee, P., Garain, U., & Pal, S. 2024, *Astrophys. J. Suppl.*, 273, 27, doi: [10.3847/1538-4365/ad5558](https://doi.org/10.3847/1538-4365/ad5558)

Shull, M., Harness, A., Trenti, M., & Smith, B. 2011, *arXiv e-prints*, arXiv:1108.3334, doi: [10.48550/arXiv.1108.3334](https://doi.org/10.48550/arXiv.1108.3334)

Simmonds, C., Tacchella, S., Hainline, K., et al. 2024, *MNRAS*, 527, 6139, doi: [10.1093/mnras/stad3605](https://doi.org/10.1093/mnras/stad3605)

Singh, S., et al. 2018, *Astrophys. J.*, 858, 54, doi: [10.3847/1538-4357/aabae1](https://doi.org/10.3847/1538-4357/aabae1)

Sohn, W., Shafieloo, A., & Hazra, D. K. 2024, *JCAP*, 03, 056, doi: [10.1088/1475-7516/2024/03/056](https://doi.org/10.1088/1475-7516/2024/03/056)

Sprenger, T., Archidiacono, M., Brinckmann, T., Clesse, S., & Lesgourgues, J. 2019, *JCAP*, 02, 047, doi: [10.1088/1475-7516/2019/02/047](https://doi.org/10.1088/1475-7516/2019/02/047)

Takezawa, K. 2006, *Introduction to Nonparametric Regression* (Hoboken, NJ: John Wiley & Sons)

Tegmark, M., & Zaldarriaga, M. 2009, *Phys. Rev. D*, 79, 083530, doi: [10.1103/PhysRevD.79.083530](https://doi.org/10.1103/PhysRevD.79.083530)

Tilvi, V., Papovich, C., Finkelstein, S. L., et al. 2014, *ApJ*, 794, 5, doi: [10.1088/0004-637X/794/1/5](https://doi.org/10.1088/0004-637X/794/1/5)

Totani, T., Kawai, N., Kosugi, G., et al. 2006, *PASJ*, 58, 485, doi: [10.1093/pasj/58.3.485](https://doi.org/10.1093/pasj/58.3.485)

van Haarlem, M. P., Wise, M. W., Gunst, A. W., et al. 2013, *A&A*, 556, A2, doi: [10.1051/0004-6361/201220873](https://doi.org/10.1051/0004-6361/201220873)

Viel, M., Becker, G. D., Bolton, J. S., & Haehnelt, M. G. 2013, *Phys. Rev. D*, 88, 043502, doi: [10.1103/PhysRevD.88.043502](https://doi.org/10.1103/PhysRevD.88.043502)

Wouthuysen, S. A. 1952, *AJ*, 57, 31, doi: [10.1086/106661](https://doi.org/10.1086/106661)

Yu, Y.-W., Cheng, K. S., Chu, M. C., & Yeung, S. 2012, *JCAP*, 2012, 023, doi: [10.1088/1475-7516/2012/07/023](https://doi.org/10.1088/1475-7516/2012/07/023)

Zaldarriaga, M., Furlanetto, S. R., & Hernquist, L. 2004, *Astrophys. J.*, 608, 622, doi: [10.1086/386327](https://doi.org/10.1086/386327)